JEM Journal of Experimental Medicine

ARTICLE

Upregulated LRRC55 promotes BK channel activation and aggravates cell injury in podocytes

Shuai Hu[1*], Runhong Han[1*], Long Chen[2*], Weisong Qin[1], Xiaodong Xu[1], Jingsong Shi[1], Xiaodong Zhu[1], Mingchao Zhang[1], Caihong Zeng[1], Zheng Tang[1], Hao Bao[1], and Zhihong Liu[1]

Podocyte injury is a common hallmark in various glomerular diseases. The level of LRRC55 was increased in podocytes of patients with focal segmental glomerulosclerosis (FSGS), diabetic nephropathy (DN), and membranous nephropathy (MN). Upregulated LRRC55 and increased intracellular Ca^{2+} led to BK channel activation and the loss of intracellular potassium, resulting in apoptosome formation and caspase-3 activation in angiotensin II (Ang II)–treated podocytes. Knockout of *Lrrc55* or the BK channel prevented the BK current and ameliorated podocyte injury in Ang II–treated mice. Upstream, NFATc3 regulated the expression of LRRC55. Increased LRRC55 expression in podocytes was also evident in animal models of FSGS, DN, and MN. Treatment with losartan or LRRC55 siRNA suppressed LRRC55 expression, prevented BK channel activation, and attenuated podocyte injury in animal models of FSGS, DN, and MN. In conclusion, upregulated LRRC55 promotes BK channel activation and aggravates cell injury in podocytes in FSGS, DN, and MN. LRRC55 inhibition may represent a new therapeutic approach for podocyte injury.

Introduction

Podocytes are a critical component of the glomerular filtration barrier and live under various stresses and pathological stimuli (Nagata, 2016). Podocyte damage is the common denominator in many forms of human and experimental glomerular diseases, such as focal segmental glomerulosclerosis (FSGS), diabetic nephropathy (DN), and membranous nephropathy (MN; Shankland, 2006). Accumulating evidence indicates that the severity of podocyte injury or loss correlates with levels of proteinuria and glomerular injury (Hanamura et al., 2014; Nagata, 2016; Xu et al., 2010). The mechanisms of podocyte injury are complex and require extensive exploration.

Leucine-rich repeat-containing (LRRC) proteins form a superfamily containing several hundred protein members. Among these proteins, LRRC55 has been reported to be a γ-subunit of the big-conductance Ca^{2+}-activated K^+ (BK) channel. The large-conductance BK channel encoded by *KCNMA1* is a unique member of the potassium channel family that is activated by membrane depolarization and elevated intracellular Ca^{2+} concentrations (Yan and Aldrich, 2012). The properties of the BK channel are altered by auxiliary subunits that do not form functional pores but alter the gating properties of KCNMA1 proteins (Lu et al., 2006). Coexpression of the auxiliary γ-subunit induces a negative shift in the voltage dependence and provides a molecular basis for activation of the BK channel at physiologic voltages and Ca^{2+} levels in nonexcitable cells (Yan and Aldrich, 2010).

The BK channel has large unitary conductance. As intracellular potassium inhibits apoptotic enzymes, the activation of a relatively small number of BK channels can have profound effects on cell physiology (Burg et al., 2006; Dryer and Reiser, 2010). Previous studies have reported that activation of the BK channel was involved in the apoptosis of NO-treated HEK293 cells and MDA-MB-231 cells (Ma et al., 2010, 2012). Krick et al. (2001) reported that the resultant potassium loss through opened BK channels serves as a trigger for cell shrinkage and caspase activation, which are major characteristics of apoptosis in pulmonary vascular smooth muscle cells. The BK channel has been detected in podocytes of mouse glomeruli and in immortalized human podocytes (Dryer and Reiser, 2010). Previously, Piwkowska et al. (2015) reported that insulin-evoked albumin permeability across podocyte monolayers was blocked by BK channel siRNA. Moreover, the BK channel inhibitor, iberiotoxin (IBTX), blocked insulin-induced disruption of the actin cytoskeleton and changes in phosphorylation in protein kinase G target proteins.

In the present study, we found that the level of LRRC55 was significantly increased in the glomerular tissues of patients with

[1]National Clinical Research Center of Kidney Diseases, Jinling Hospital, Nanjing University School of Medicine, Nanjing, China; [2]National Standard Laboratory of Pharmacology for Chinese Materia Medica, School of Pharmacy, Nanjing University of Chinese Medicine, Nanjing, China.

*S. Hu, R. Han, and L. Chen contributed equally to this paper; Correspondence to Zhihong Liu: zhliunj@vip.163.com; Hao Bao: bhao@nju.edu.cn.

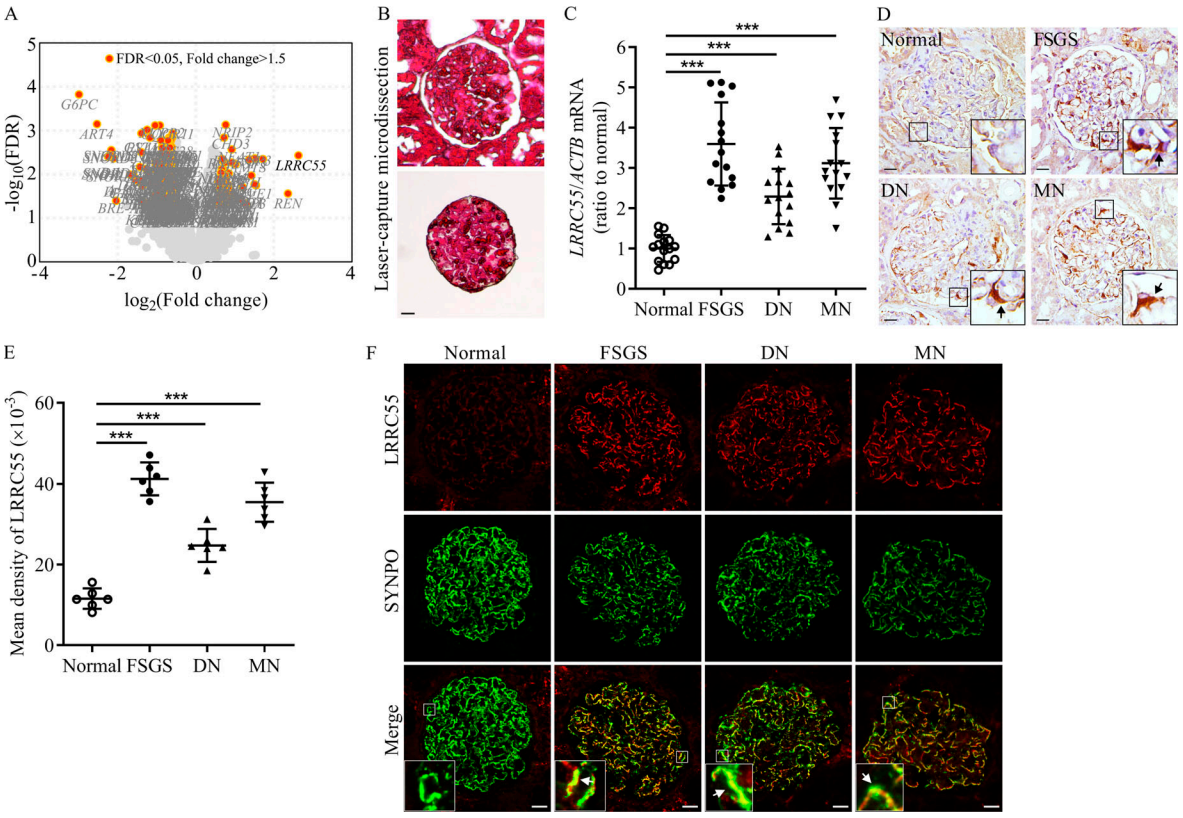

Figure 1. **Expression of LRRC55 in glomerular tissues of FSGS, DN, and MN patients. (A)** Volcano plot of differentially expressed genes in glomerular tissues of FSGS patients and normal controls (n = 5). **(B)** Isolation of glomerular tissues by laser capture microdissection. **(C)** The level of *LRRC55* mRNA in glomerular tissues of patients with FSGS, DN, and MN (n = 15, validation cohort). **(D)** IHC analysis of LRRC55 in glomerular tissues of patients with FSGS, DN, and MN. Black arrows indicate positive staining of LRRC55. **(E)** Quantification of LRRC55 expression levels in glomerular tissues (n = 6). **(F)** Coexpression staining of LRRC55 and synaptopodin (SYNPO) in glomerular tissues of patients with FSGS, DN, and MN. White arrows show regions of superimposition of LRRC55 and SYNPO. Data shown are representative of one (A) or three (B–F) experiments. For statistical analysis, one-way ANOVA with Tukey's post hoc test was used for C and E. ***, P < 0.001. Scale bar = 20 µm. FDR, false discovery rate.

FSGS, DN, and MN. The level of LRRC55 has also been shown to be increased in the glomerular tissues of patients with FSGS and MN compared with tissue of other nephrotic syndrome patients in a transcriptomic analysis reported by the NEPTUNE study (Sampson et al., 2016). The role of LRRC55 in podocyte injury and glomerular disease has not been explored. Based on our findings and a literature review, we hypothesized that LRRC55 overexpression may lead to podocyte injury by activating the BK channel in podocytes in glomerular disease. In the study, we conducted both in vitro and in vivo experiments to investigate the role of LRRC55 in podocyte injury.

Results

Increased expression of LRRC55 in podocytes in human glomerular disease

Renal glomerular tissues from five FSGS patients and five normal controls were microdissected, and an Affymetrix HTA 2.0 microarray was used to perform a global analysis of the gene expression patterns in tissues (Fig. 1 A). The level of *LRRC55* mRNA showed a significant increase in the glomerular tissues of FSGS patients (Fig. 1 A). PCR analysis of another set of patients confirmed the increased level of *LRRC55* mRNA in the glomerular tissues of patients with FSGS (Fig. 1, B and C). In addition, we also found an increase in the *LRRC55* mRNA level in the glomerular tissues of patients with DN or MN (Fig. 1 C). By contrast, no increase in LRRC55 level was detected in the glomerular tissues of patients with interstitial nephritis or minimal change disease (MCD; Fig. S1). Immunohistochemical (IHC) staining showed that LRRC55 was weakly positive in the glomeruli of normal controls, while in FSGS, DN, and MN patients, the level of LRRC55 was significantly increased in the injured glomeruli, particularly in the area of sclerotic segments (Fig. 1, D and E). Immunofluorescence staining confirmed that LRRC55 expression was upregulated and colocalized with synaptopodin in glomerular tissue of patients with FSGS, DN, and MN (Fig. 1 F).

Knockout of *Lrrc55* ameliorates podocyte injury in angiotensin II (Ang II)–treated mice

Abnormal activation of the renin-angiotensin system has been implicated in FSGS, DN, and MN by several studies (Bahiense-Oliveira et al., 2010; Batlle et al., 2012; Mezzano et al., 2003; Nijenhuis et al., 2011). An Ang II–induced podocyte injury model was generated by subjecting mice to Ang II infusions at a dose of 1,000 ng/kg/min for 28 d. mRNA and protein levels of LRRC55

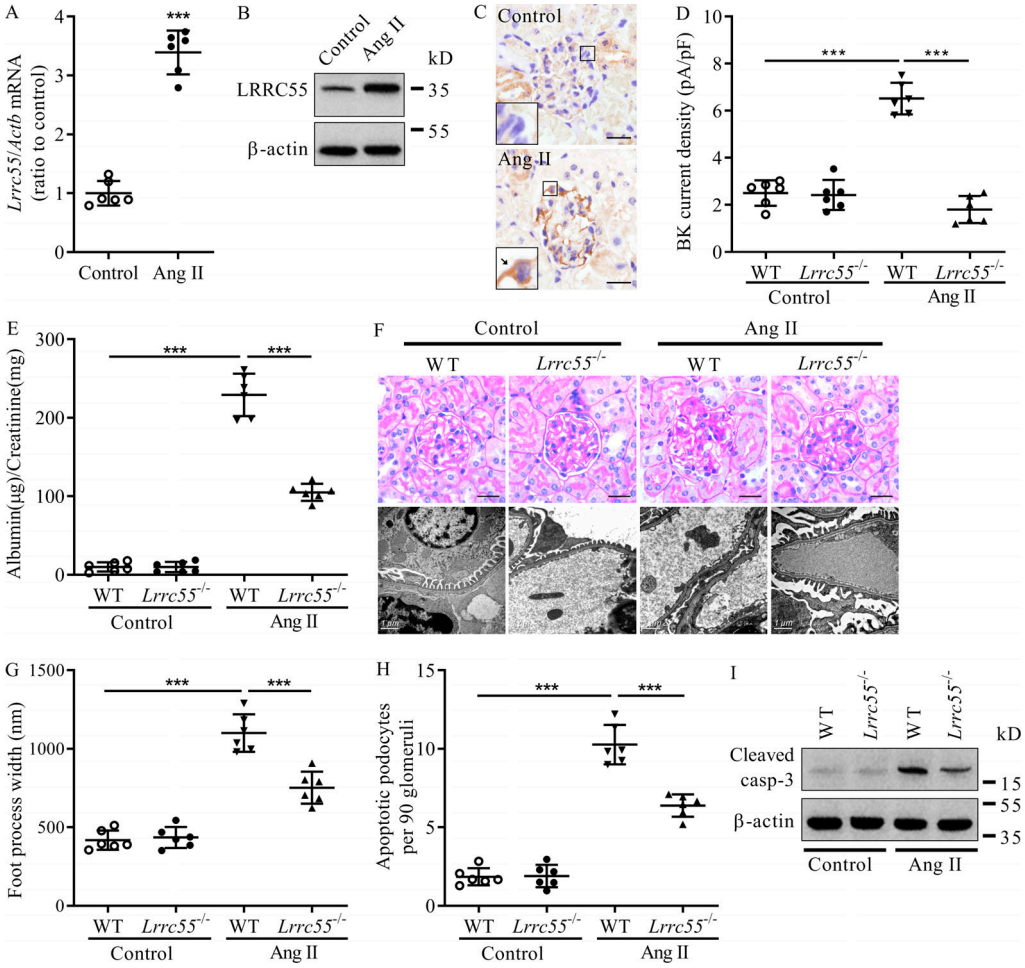

Figure 2. **Knockout of *Lrrc55* ameliorates podocyte injury in Ang II–induced mice. (A and B)** RT-PCR and Western blot analysis of LRRC55 in podocytes of mice treated with Ang II (n = 6). Mice glomeruli were isolated by using the magnetic bead–based isolation technique, single-cell suspensions were obtained with enzymatic disaggregation, and then podocytes were enriched by using anti-podocalyxin beads for RT-PCR and Western blot analysis. **(C)** IHC analysis of LRRC55 in glomerular tissues of mice treated with Ang II (n = 6). Black arrow indicates positive staining for LRRC55. **(D)** The BK current measured at +80 mV in podocytes of freshly isolated glomeruli from mice treated with Ang II (n = 6). To analyze the whole-cell recording of the BK current in situ, the isolated glomeruli were attached to poly-L-lysine–coated coverslips, and then the coverslips were placed into a patch-clamp chamber and perfused with bath solution to conduct a patch-clamp experiment. **(E)** Urinary albumin excretion of mice treated with Ang II (n = 6). **(F)** Periodic acid–Schiff staining and electron microscopy analysis of renal sections. **(G)** Mean width of podocyte foot processes (n = 6). **(H)** The number of apoptotic podocytes in glomerular tissues of mice treated with Ang II (n = 6). **(I)** Western blot analysis of cleaved caspase-3 (casp-3) in glomerular tissues of mice treated with Ang II. Data shown are representative of three experiments. For statistical analysis, a two-tailed Student's t test was used for A, and one-way ANOVA with Tukey's post hoc test was used for D, E, G, and H. ***, P < 0.001. Scale bar = 20 μm, unless otherwise indicated.

were increased in glomerular podocytes from Ang II–treated mice (Fig. 2, A and B). IHC staining confirmed that LRRC55 expression was upregulated in podocytes from Ang II–treated mice (Fig. 2 C).

LRRC55 has been reported to be a γ-subunit of the BK channel (Yan and Aldrich, 2012). To analyze whole-cell recordings of the BK current in situ, isolated mouse glomeruli were attached to poly-L-lysine–coated coverslips, and then the coverslips were placed into a patch-clamp chamber and perfused with bath solution to conduct a patch-clamp experiment (Fig. S2). BK current was found to be significantly increased in podocytes from Ang II–treated mice compared with controls (Fig. 2 D). Knockout of *Lrrc55* inhibited the activation of the BK channel in podocytes from the Ang II–treated mice (Fig. 2 D). *Lrrc55* knockout also significantly attenuated the rate of urinary albumin excretion in Ang II–treated mice (Fig. 2 E). Periodic acid–Schiff staining and electron microscopy analysis revealed that Ang II–induced focal segmental lesions and foot process effacement were attenuated in the kidneys of *Lrrc55* knockout mice (Fig. 2, F and G). Immunofluorescence staining and Western blot analysis showed that the number of apoptotic podocytes and caspase-3 activity were decreased in *Lrrc55* knockout mice treated with Ang II (Fig. 2, H and I).

Upregulated LRRC55 and increased intracellular Ca^{2+} contribute to Ang II–induced BK channel activation in podocytes

We treated immortalized human podocytes with different doses of Ang II for different durations in vitro. Ang II treatment increased LRRC55 expression in both a dose- and time-dependent

manner (Fig. 3, A–D). No effect of Ang II on the expression of *KCNMA1* or other γ-subunits was detected (Fig. 3 E).

In Ang II–treated podocytes, the BK current was increased after treatment with 1 µM Ang II for 24 h. siRNA was transfected to knock down LRRC55 expression in podocytes, and the efficiency was confirmed by using Western blotting (Fig. S3 A). As shown by the results, the silencing of LRRC55 prevented the activation of the BK channel in Ang II–treated podocytes (Fig. 3, F and G). Interestingly, the BK current was not increased in podocytes that were only transfected with LRRC55 expression plasmid (Fig. 3 H and Fig. S3 B).

The BK channel is a Ca^{2+}-sensing channel, and TRPC6 is a key channel responsible for Ca^{2+} influx in Ang II–treated podocytes (Ilatovskaya and Staruschenko, 2015; Schreiber and Salkoff, 1997). We analyzed the Ca^{2+} influx in podocytes with the Ca^{2+} indicator, Fluo-4 AM. The addition of Ang II to podocytes induced Ca^{2+} influx within several minutes (Fig. 3, I and J). The silencing of TRPC6 prevented the activation of the BK channel in podocytes that were treated with Ang II for 24 h, which was similar to the effect of LRRC55 siRNA (Fig. 3 K and Fig. S3 C). Conversely, although Ang II alone did not activate the BK channel within 4 min, short-term treatment activated the BK channel in LRRC55-overexpressing podocytes, and silencing of TRPC6 reversed this effect (Fig. 3 L). In addition, treatment with the BK channel activator, NS1619, also caused the activation of the TRPC6 channel and Ca^{2+} influx in podocytes (Fig. S4, A–C). The inhibition of the BK channel with IBTX or the silencing of LRRC55 attenuated the TRPC6 current and intracellular Ca^{2+} in podocytes treated with Ang II (Fig. S4, D–G). These data suggest that LRRC55 overexpression and Ca^{2+} influx contribute to Ang II–induced BK channel activation, which aggravates TRPC6-mediated Ca^{2+} influx in podocytes.

Decreased intracellular potassium induces cell apoptosis in podocytes

We measured intracellular potassium with a cell-permeable, potassium-sensitive fluorescence probe (potassium-binding benzofuran isophthalate [PBFI]–AM). Following activation of the BK channel, Ang II treatment decreased intracellular potassium level in podocytes (Fig. 4 A). Experiments involving activated cell extracts showed that potassium inhibited apoptosome formation and caspase-3 activation in a concentration-dependent manner, and nearly complete suppression was observed with 130 mM KCl (Fig. 4, B and C). Thus, the physiologic concentration of potassium directly inhibited apoptosome formation and caspase-3 activation, whereas lower concentrations of potassium induced apoptosome formation and caspase-3 activation. High concentrations of potassium prevented DNA fragmentation, whereas low concentrations of potassium caused obvious DNA fragmentation in activated cell extracts (Fig. 4 D).

Ang II treatment promoted apoptosome formation, caspase-3 activation, and DNA fragmentation in podocytes, mimicking the effect of the BK channel activator, NS1619 (Fig. 4, E–G). In contrast, the silencing of LRRC55 reversed apoptosome formation, caspase-3 activation, and DNA fragmentation in Ang II–treated podocytes. LRRC55 silencing also decreased cell apoptosis in podocytes treated with Ang II (Fig. 4, H and I).

Knockout of the BK channel ameliorates podocyte injury in Ang II–treated mice

As Ang II induced an increase in the BK current in podocytes from Ang II–treated mice, *Kcnma1* knockout mice were used to observe the effect of the BK channel on podocyte injury. Mouse glomeruli were isolated by using the magnetic bead–based isolation technique, and whole-cell recordings of the BK current and intracellular potassium were measured in podocytes of glomeruli in situ. Knockout of *Kcnma1* abolished the Ang II–induced BK current and prevented the decrease in intracellular potassium in podocytes from Ang II–treated mice (Fig. 5, A and B). Knockout of *Kcnma1* also reduced caspase-3 activity and apoptotic podocytes in glomerular tissues from Ang II–treated mice (Fig. 5, C and D). Consequently, Ang II–induced proteinuria, focal segmental sclerosis, and foot process effacement were ameliorated in *Kcnma1* knockout mice (Fig. 5, E–G).

Ang II promotes LRRC55 expression by stimulating NFATc3 nuclear translocation

A promoter-binding transcription factor (TF) profiling plate array was performed to identify TFs that may bind to the *LRRC55* promoter region. Of the scanned transcriptional factors, six factors could bind to the promoter sequence of *LRRC55* (Fig. 6 A). We knocked down their expression levels with siRNAs and found that knockdown of NFATc3, but not other factors, significantly inhibited the expression of *LRRC55* in podocytes treated with Ang II (Fig. 6 B).

Western blot and immunofluorescence staining showed that treatment with Ang II induced nuclear translocation of NFATc3 in podocytes (Fig. 6, C and D). We scanned the DNA sequence of the *LRRC55* promoter and identified two binding sites for NFATc3 (Fig. 6 E). Chromatin immunoprecipitation (ChIP) analysis showed that NFATc3 bound to the *LRRC55* promoter in the podocytes, and this binding was enhanced by Ang II treatment (Fig. 6 F). Overexpression of NFATc3 increased the expression of luciferase reporter constructs containing the binding sequence. Site-directed mutations rescued the NFATc3-mediated upregulation of the *LRRC55* promoter–luciferase reporter plasmid (Fig. 6, G and H).

NFATc3 overexpression also increased endogenous LRRC55 expression at both the mRNA and protein level in podocytes (Fig. 6, I and J). Conversely, knockdown of NFATc3 suppressed Ang II–induced LRRC55 expression (Fig. 6, K and L). Based on these observations, NFATc3 regulated LRRC55 expression in podocytes treated with Ang II.

Inhibition of NFATc3 suppresses LRRC55 expression in podocytes of Ang II–treated mice

Immunofluorescence staining of renal tissues showed that the nuclear accumulation of NFATc3 was increased in renal podocytes from Ang II–treated mice (Fig. 7 A). Treatment with the NFAT-specific inhibitor, 11R-VIVIT, attenuated the nuclear accumulation of NFATc3 and prevented the increase in LRRC55 in podocytes from Ang II–treated mice (Fig. 7, A–C). Activation of the BK channel and the decrease in intracellular potassium were suppressed in podocytes from Ang II–induced mice treated with 11R-VIVIT (Fig. 7, D and E). Caspase-3 activity and the number of

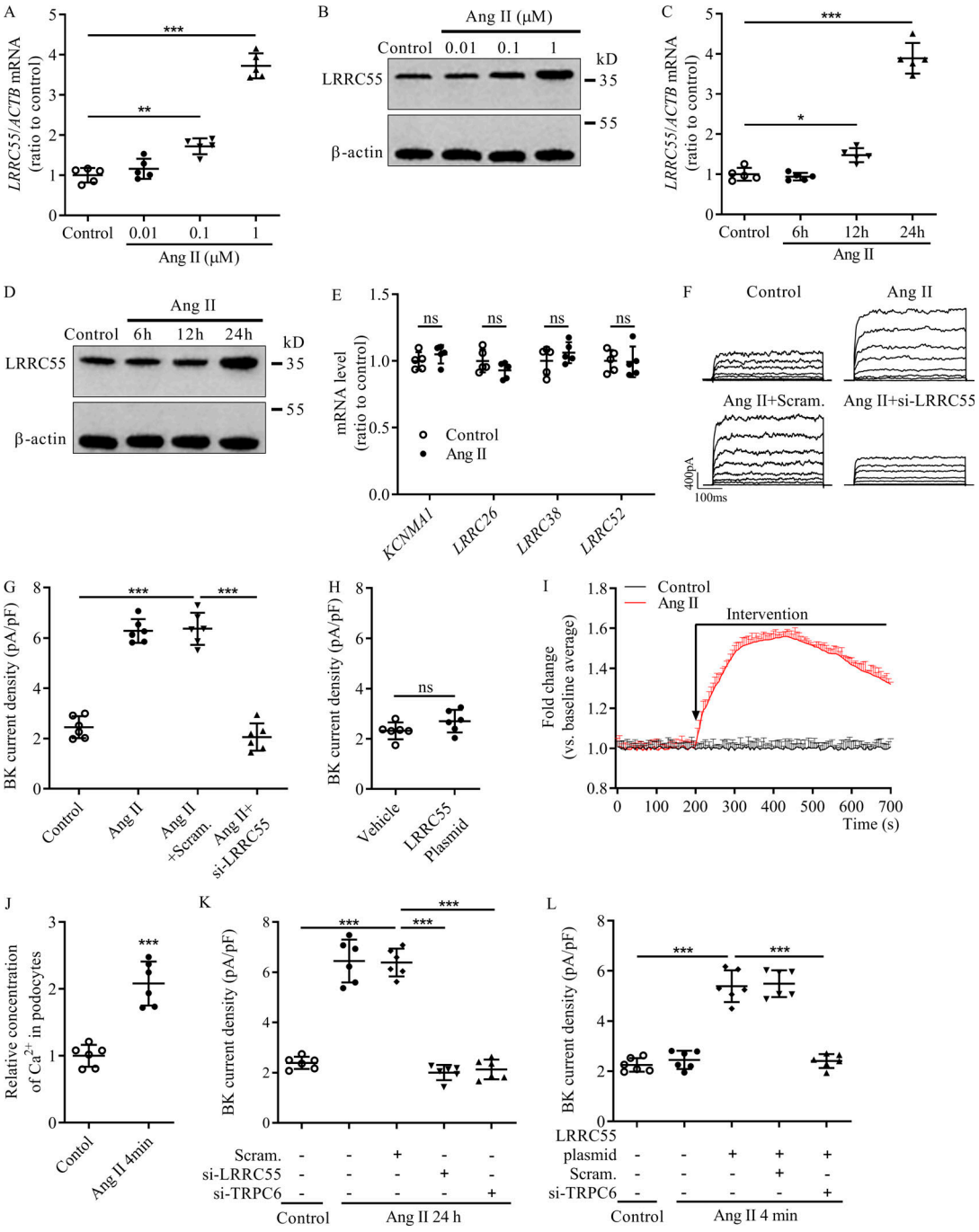

Figure 3. **Ang II activates the BK channel by upregulating LRRC55 and Ca^{2+} influx in podocytes. (A)** The level of *LRRC55* mRNA in podocytes treated with different doses of Ang II for 24 h (n = 5). **(B)** Western blot analysis of LRRC55 in podocytes treated with different doses of Ang II for 24 h (n = 3). **(C)** The level of *LRRC55* mRNA in podocytes treated with Ang II (1 μM) for different durations (n = 5). **(D)** Western blot analysis of LRRC55 in podocytes treated with Ang II (1 μM) for different durations (n = 3). **(E)** Levels of *KCNMA1*, *LRRC26*, *LRRC38*, and *LRRC52* mRNA in podocytes treated with Ang II (1 μM) for 24 h (n = 5). **(F)** Representative traces of the whole-cell BK current in podocytes treated with Ang II (1 μM) and LRRC55 siRNA (15 nM) for 24 h. **(G)** The BK current measured at +80 mV in podocytes treated with Ang II and LRRC55 siRNA for 24 h (n = 6). **(H)** The BK current measured at +80 mV in podocytes transfected with the LRRC55 expression plasmid for 24 h (n = 6). **(I)** Representative transients of intracellular Ca^{2+} dynamics in podocytes treated with Ang II (1 μM). To analyze Ca^{2+} influx, cells were incubated with the Ca^{2+} indicator, Fluo-4 AM, and then fluorescence images were captured every 5 s. Changes in intracellular Ca^{2+} levels were estimated from the fluorescence images as previously described (Ilatovskaya et al., 2015a). **(J)** The level of intracellular Ca^{2+} in podocytes treated with Ang II (1 μM) for 4 min (n = 6). **(K)** The effect of TRPC6 siRNA and LRRC55 siRNA on the BK current in podocytes treated with Ang II (1 μM) for 24 h (n = 6). **(L)** Effect of LRRC55 overexpression and TRPC6 siRNA on the BK current in podocytes treated with Ang II (1 μM) for 4 min (n = 6). Data shown are representative of three experiments. For statistical analysis, a two-tailed Student's t test was used for E, H, and J, and one-way ANOVA with Tukey's post hoc test was used for A, C, G, K, and L. *, P < 0.05; **, P < 0.01; ***, P < 0.001; ns, not significant. Scram., scrambled.

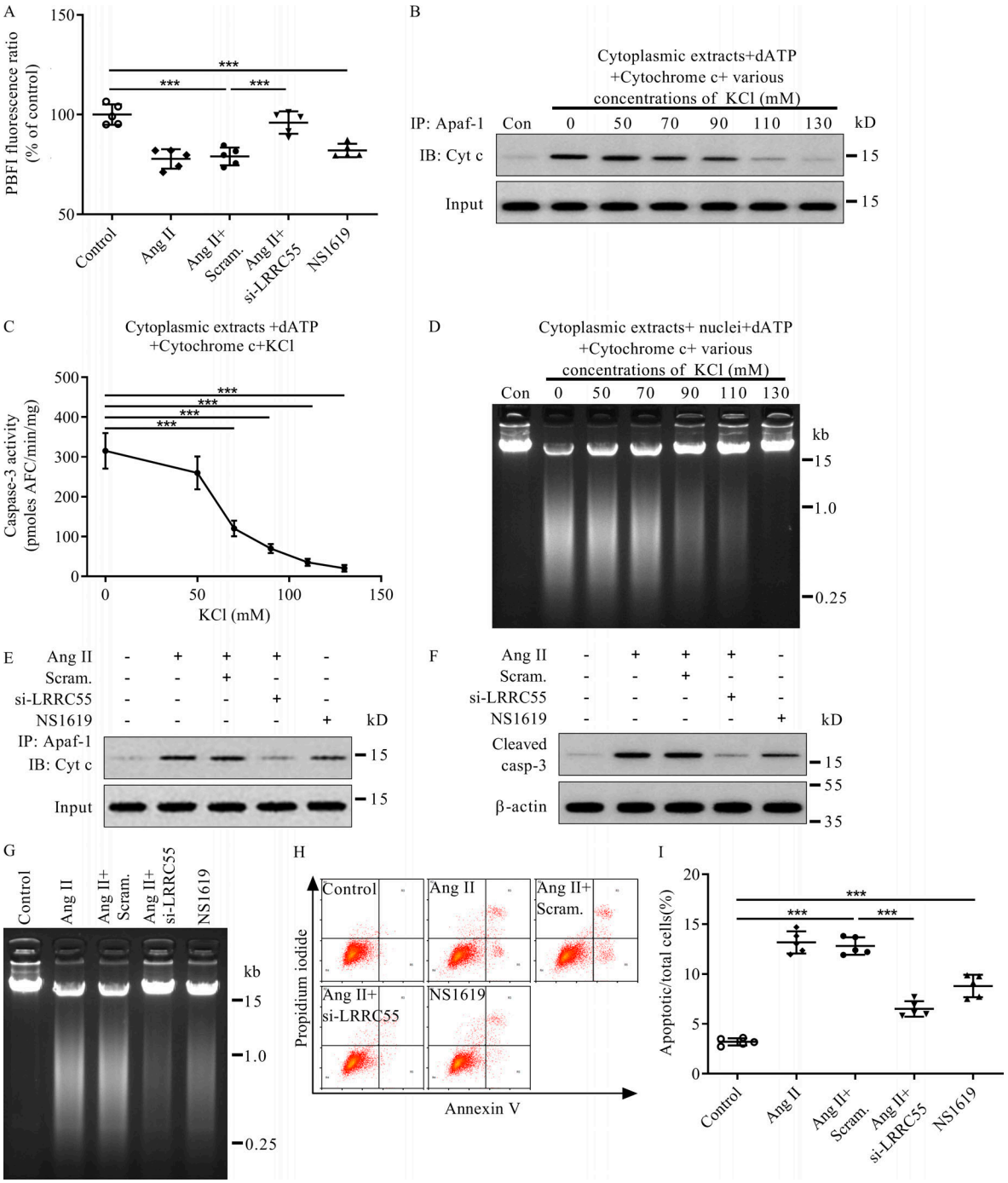

Figure 4. **Decreased intracellular potassium induces cell apoptosis in podocytes. (A)** Level of intracellular potassium in podocytes treated with Ang II (1 µM), LRRC55 siRNA, or NS1619 (30 µM) for 24 h (n = 5). **(B)** Immunoprecipitation (IP) analysis of the binding between Apaf-1 and cytochrome c (Cyt c) in cytoplasmic extracts incubated with dATP (1 mM), cytochrome c (10 µg/ml), and decreasing concentrations of KCl (n = 3). **(C)** Changes in caspase-3 activity in cytoplasmic extracts incubated with dATP, cytochrome c, and decreasing concentrations of KCl (n = 5). **(D)** Gel analysis of DNA fragmentation in the mixture of cytoplasmic extracts, nuclei, dATP, cytochrome c, and decreasing concentrations of KCl (n = 3). **(E)** IP analysis of the binding between Apaf-1 and cytochrome c in podocytes treated with Ang II, LRRC55 siRNA, or NS1619 for 24 h (n = 3). **(F)** Western blot analysis of cleaved caspase-3 (casp-3) in podocytes treated with Ang II, LRRC55 siRNA, or NS1619 for 24 h (n = 3). **(G)** Gel analysis of DNA fragmentation in podocytes treated with Ang II, LRRC55 siRNA, or NS1619 for 24 h (n = 3). **(H and I)** Flow cytometric analysis of apoptotic cells among podocytes (n = 5). Data shown are representative of three experiments. For statistical analysis, one-way ANOVA with Tukey's post hoc test was used for A, C, and I. ***, P < 0.001. AFC, 7-amino-4-trifluoromethylcoumarin; IB, immunoblotting; Scram., scrambled.

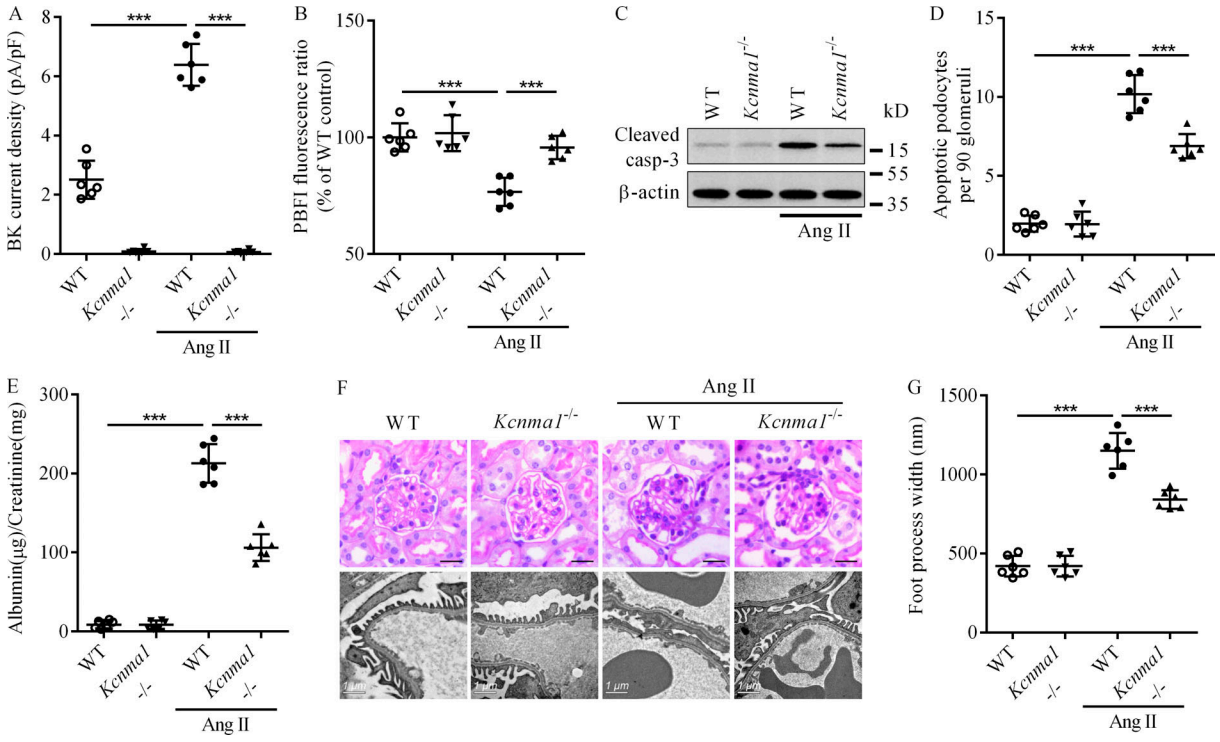

Figure 5. **Effect of BK channel knockout on podocyte injury in Ang II–treated mice. (A)** The BK current measured at +80 mV in podocytes of freshly isolated glomeruli from WT and *Kcnma1*$^{-/-}$ mice treated with Ang II (n = 6). **(B)** The level of intracellular potassium in podocytes of freshly isolated glomeruli from mice (n = 6). To analyze intracellular potassium in podocytes of mouse glomeruli in situ, isolated glomeruli were incubated with 10 μM PBFI-AM, 0.04% Pluronic F-127, and PE-conjugated podocalyxin antibody (1:200) for 40 min at room temperature. The glomeruli were then attached to poly-L-lysine–coated glass coverslips. Fluorescence images were acquired by using a Zeiss LSM710 confocal microscope. PBFI fluorescence intensities in podocalyxin-positive cells were analyzed to determine the intracellular potassium level in podocytes of mouse glomeruli. **(C)** Western blot analysis of cleaved caspase-3 (casp-3) in glomerular tissues of mice (n = 6). **(D)** Apoptotic podocytes in mouse glomeruli (n = 6). **(E)** Urinary albumin excretion in WT and *Kcnma1*$^{-/-}$ mice treated with Ang II (n = 6). **(F)** Periodic acid–Schiff staining and electron microscopy analysis of renal sections. **(G)** Mean width of podocyte foot processes (n = 6). Data shown are representative of three experiments. For statistical analysis, one-way ANOVA with Tukey's post hoc test was used for A, B, D, E, and G. ***, $P < 0.001$. Scale bar = 20 μm, unless otherwise indicated.

apoptotic podocytes were decreased in Ang II–induced mice treated with 11R-VIVIT (Fig. 7, F and G). Consequently, Ang II–induced proteinuria, focal segmental sclerosis, and foot process effacement were inhibited by 11R-VIVIT treatment (Fig. 7, H–J).

Treatment with losartan prevents LRRC55 expression and ameliorates podocyte injury in adriamycin (ADR) nephropathy, DN, and passive Heymann nephritis (PHN)

As LRRC55 expression was increased in the renal podocytes of patients with FSGS, DN, and MN, we examined LRRC55 expression in ADR-treated mice, diabetic mice, and PHN rats. The level of LRRC55 was significantly increased in the podocytes of ADR-treated mice, diabetic mice, and PHN rats (Fig. 8, A and B; Fig. 9, A and B; and Fig. 10, A and B). IHC staining showed that LRRC55 was weakly positive in the glomeruli of control mice and rats. In ADR-treated mice, diabetic mice, and PHN rats, the level of LRRC55 was significantly increased in the injured glomeruli (Fig. 8 C, Fig. 9 C, and Fig. 10 C). Treatment with the angiotensin receptor blocker, losartan, or LRRC55 siRNA prevented the increase in LRRC55 expression and attenuated the activation of the BK channel and the decrease in intracellular potassium in podocytes from ADR-treated mice, diabetic mice, and PHN rats (Fig. 8, A–E; Fig. 9, A–E; and Fig. 10, A–E). Treatment with losartan or LRRC55 siRNA also reduced caspase-3 activity and apoptotic podocytes in glomerular tissues from ADR-treated mice, diabetic mice, and PHN rats (Fig. 8, F and G; Fig. 9, F and G; and Fig. 10, F and G). As expected, the proteinuria level and foot process effacement were decreased in ADR-treated mice, diabetic mice, and PHN rats that were treated with losartan or LRRC55 siRNA (Fig. 8, H–J; Fig. 9, H–J; and Fig. 10, H–J).

Discussion

Podocytes are highly specialized cells that wrap around glomerular capillaries and constitute a key component of the glomerular filtration barrier. We found that the level of LRRC55 was increased in the podocytes of patients with FSGS, DN, and MN, and knockout of *Lrrc55* ameliorated podocyte injury in Ang II–treated mice. Increased levels of LRRC55 were also evident in podocytes from animal models of FSGS, DN, and MN, and treatment with losartan or the silencing of LRRC55 decreased LRRC55 expression and attenuated podocyte injury in the animal models of FSGS, DN, and MN. In contrast, the level of LRRC55 was not changed in the glomerular tissues of interstitial nephritis patients without proteinuria or MCD patients with heavy proteinuria, but no progressive glomerular injury.

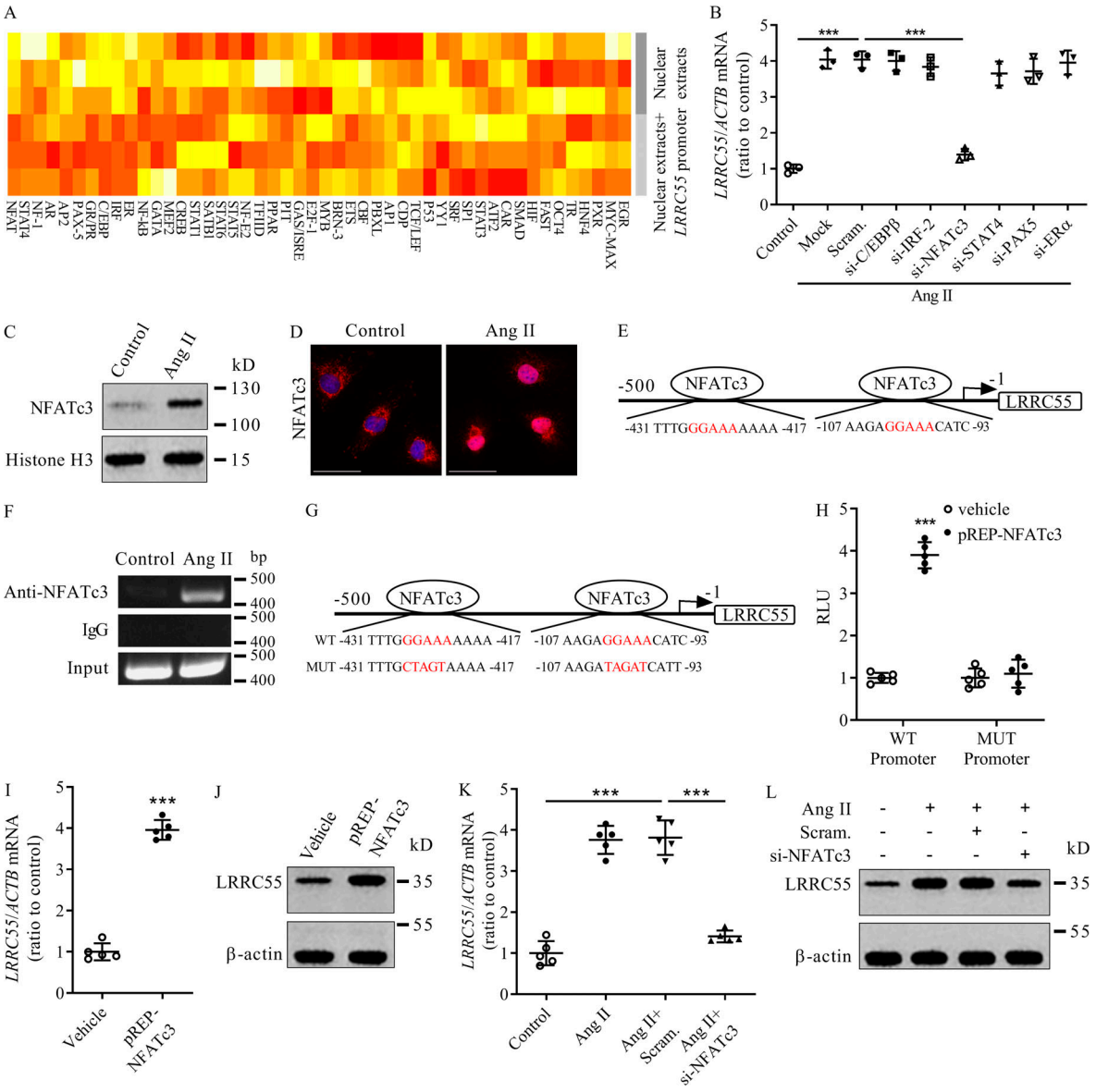

Figure 6. **NFATc3 binds to the *LRRC55* promoter and induces LRRC55 overexpression. (A)** Screening of TFs binding to the *LRRC55* promoter using a promoter-binding TF profiling plate array (n = 3). Podocytes were treated with Ang II for 24 h to activate TFs. Nuclear extracts were prepared and incubated with TF binding oligo probe mix with or without an *LRRC55* promoter DNA fragment. After spin separation of complexes from unbound free biotin-labeled oligos, TF-bound probes were eluted from the column and used for hybridization and analysis. **(B)** The level of *LRRC55* mRNA in podocytes treated with Ang II, C/EBPβ siRNA, IRF-2 siRNA, NFATc3 siRNA, STAT4 siRNA, PAX5 siRNA, and ERα siRNA (n = 3). **(C)** Western blot analysis of nuclear NFATc3 in podocytes treated with Ang II (1 µM) for 24 h (n = 3). **(D)** Immunofluorescence staining of nuclear NFATc3 in podocytes treated with Ang II (1 µM) for 24 h (n = 3). **(E)** Schematic of the NFATc3 binding sites in the upstream sequence of the *LRRC55* promoter. **(F)** ChIP analysis of the binding between NFATc3 and the *LRRC55* promoter in podocytes treated with Ang II (1 µM) for 24 h (n = 3). **(G)** Schematic of the WT and mutated (MUT) *LRRC55* promoter-luciferase reporter plasmids. **(H)** Normalized luciferase activity of reporter constructs in podocytes cotransfected with NFATc3 plasmid for 24 h (n = 5). **(I)** RT-PCR analysis of *LRRC55* in podocytes transfected with NFATc3 plasmid for 24 h (n = 5). **(J)** Western blot analysis of LRRC55 in podocytes transfected with NFATc3 plasmid (n = 3). **(K)** RT-PCR analysis of *LRRC55* in podocytes treated with Ang II (1 µM) and NFATc3 siRNA for 24 h (n = 5). **(L)** Western blot analysis of LRRC55 in podocytes treated with Ang II (1 µM) and NFATc3 siRNA for 24 h (n = 3). Data shown are representative of three experiments. For statistical analysis, one-way ANOVA with Tukey's post hoc test was used for B and K, and a two-tailed Student's t test was used for H and I. ***, $P < 0.001$. Scale bar = 20 µm. Scram., scrambled.

Although MCD is a characteristic disease of podocytopathy, podocytes are mildly damaged and maintain normal podocyte numbers in MCD patients (Nakamura et al., 2000; Wiggins, 2007). These findings are consistent with the data reported by Sampson et al. (2016), who showed that the level of *LRRC55* mRNA was increased in glomerular tissues of patients with FSGS and MN compared with patients with other nephrotic syndromes in their transcriptomic analysis. The level of *LRRC55* has also been shown to be increased in the renal tissues of patients with chronic kidney disease compared with normal controls in the transcriptomic analysis conducted by Nakagawa et al. (2015).

LRRC55 is one of the four γ-subunits of the BK channel responsible for modulating the voltage dependence of BK channel

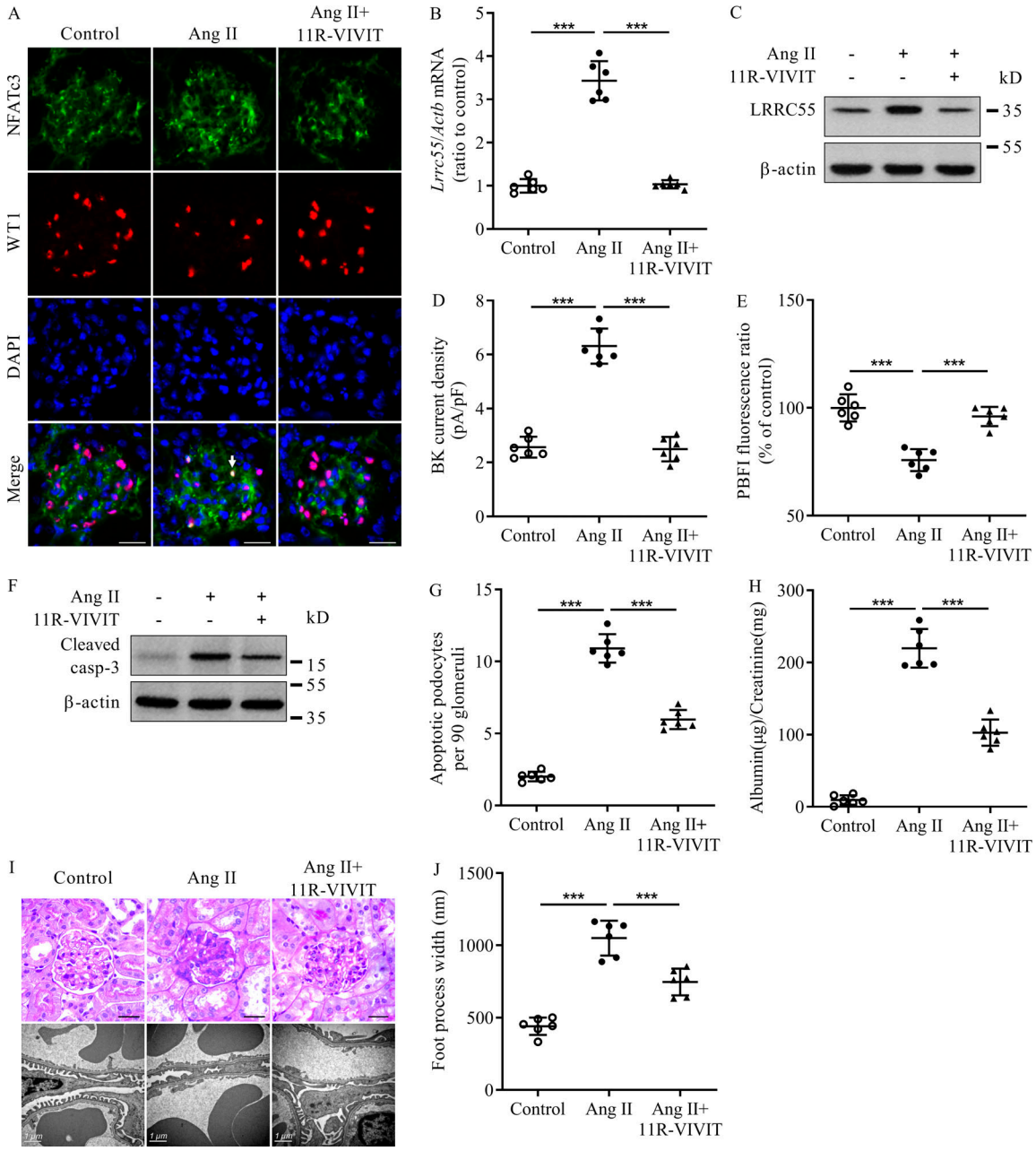

Figure 7. **Effect of NFATc3 inhibition on podocyte injury in Ang II–treated mice. (A)** Nuclear accumulation of NFATc3 in podocytes of mice treated with Ang II and 11R-VIVIT. White arrow indicates nuclear accumulation of NFATc3 in the podocytes. **(B)** The level of *Lrrc55* mRNA in the podocytes of mice (n = 6). **(C)** The level of LRRC55 protein in the podocytes of mice (n = 6). **(D)** The BK current measured at +80 mV in podocytes of freshly isolated glomeruli from mice treated with Ang II and 11R-VIVIT (n = 6). **(E)** The level of intracellular potassium in podocytes of freshly isolated glomeruli from mice (n = 6). **(F)** Western blot analysis of cleaved caspase-3 (casp-3) in glomerular tissues of mice treated with Ang II and 11R-VIVIT (n = 6). **(G)** Apoptotic podocytes in glomerular tissues of mice treated with Ang II and 11R-VIVIT (n = 6). **(H)** Urinary albumin excretion in mice treated with Ang II and 11R-VIVIT (n = 6). **(I)** Periodic acid–Schiff staining and electron microscopy analysis of renal sections. **(J)** Mean width of podocyte foot processes in mice treated with Ang II and 11R-VIVIT (n = 6). Data shown are representative of three experiments. For statistical analysis, one-way ANOVA with Tukey's post hoc test was used for B, D, E, G, H, and J. ***, $P < 0.001$. Scale bar = 20 µm, unless otherwise indicated.

activation and exhibits tissue-specific expression patterns (Zhang and Yan, 2014). The properties of the BK channel are altered by auxiliary subunits that do not form functional pores but alter the gating properties of KCNMA1 proteins (Lu et al., 2006). We found that the overexpression of LRRC55 alone was not sufficient to induce a BK current; however, LRRC55 overexpression activated BK channels in the presence of Ca^{2+} influx. Our result is consistent with that of a previous report showing that, although each of the four BK γ-proteins shifts the voltage dependence of BK channel activation in a hyperpolarizing direction, they show markedly different efficacies (Li et al., 2015). LRRC26 causes a large negative shift, which opens BK channels at near-physiologic Ca^{2+} concentrations and membrane voltage in nonexcitable cells, while LRRC55 opens BK channels only in

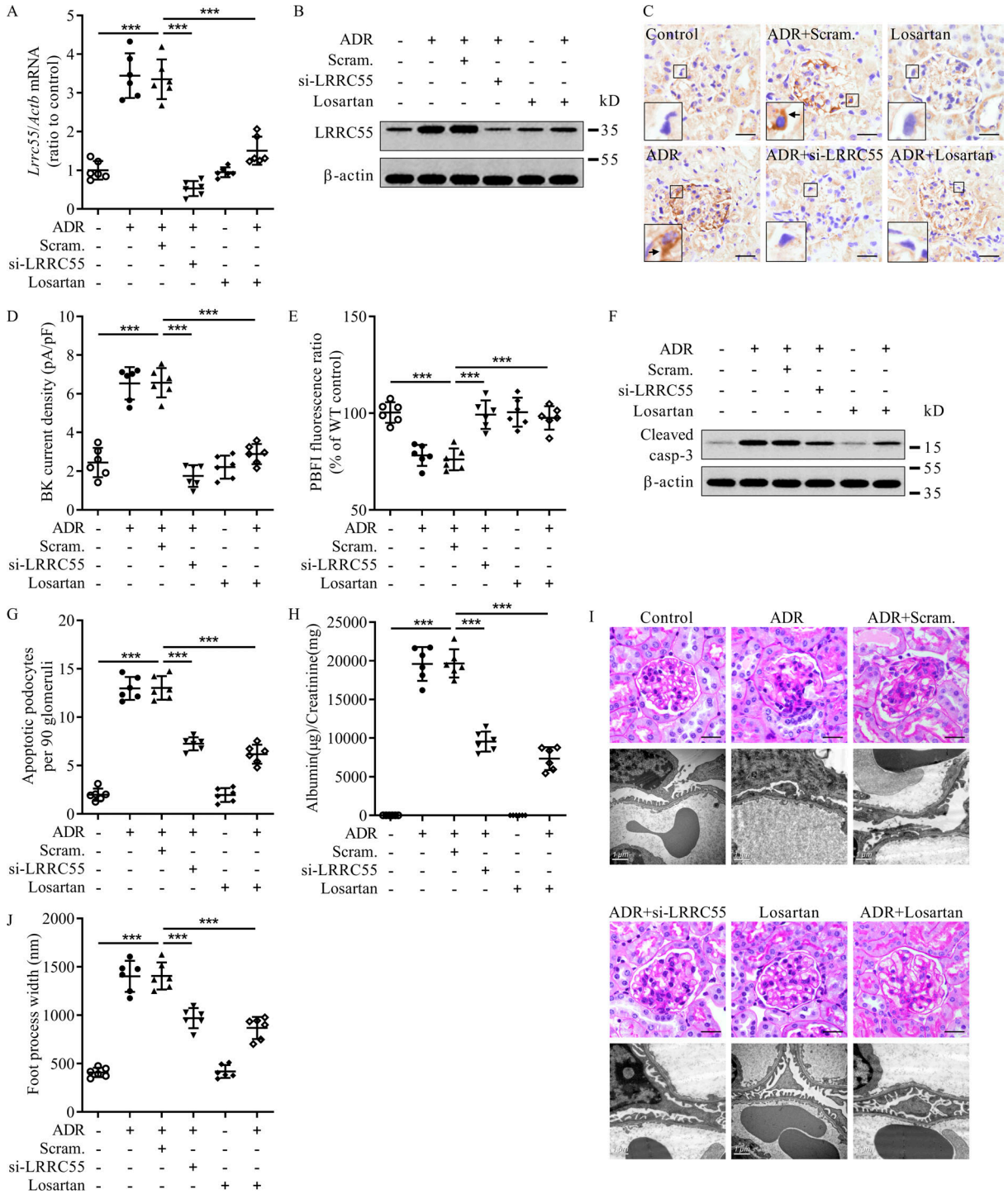

Figure 8. **Effects of losartan on LRRC55 expression and podocyte injury in ADR-treated mice. (A)** The level of *Lrrc55* mRNA in podocytes of ADR-treated mice treated with losartan or LRRC55 siRNA (n = 6). **(B)** Western blot analysis of LRRC55 expression in podocytes of ADR-treated mice (n = 6). **(C)** IHC analysis of LRRC55 expression in the renal tissues of ADR-treated mice (n = 6). Black arrows indicate positive staining of LRRC55. **(D)** The BK current measured at +80 mV in podocytes of freshly isolated glomeruli from ADR-treated mice (n = 6). **(E)** Intracellular potassium levels in podocytes of freshly isolated glomeruli from ADR-treated mice (n = 6). **(F)** Western blot analysis of cleaved caspase-3 (casp-3) in glomerular tissues of ADR-treated mice (n = 6). **(G)** The number of apoptotic podocytes in glomerular tissues of ADR-treated mice (n = 6). **(H)** Urinary albumin excretion of ADR-treated mice (n = 6). **(I)** Periodic acid–Schiff staining and electron microscopy analysis of renal sections. **(J)** Mean width of podocyte foot processes (n = 6). Data shown are representative of three experiments. For statistical analysis, one-way ANOVA with Tukey's post hoc test was used for A, D, E, G, H, and J. ***, P < 0.001. Scale bar = 20 μm, unless otherwise indicated. Scram., scrambled.

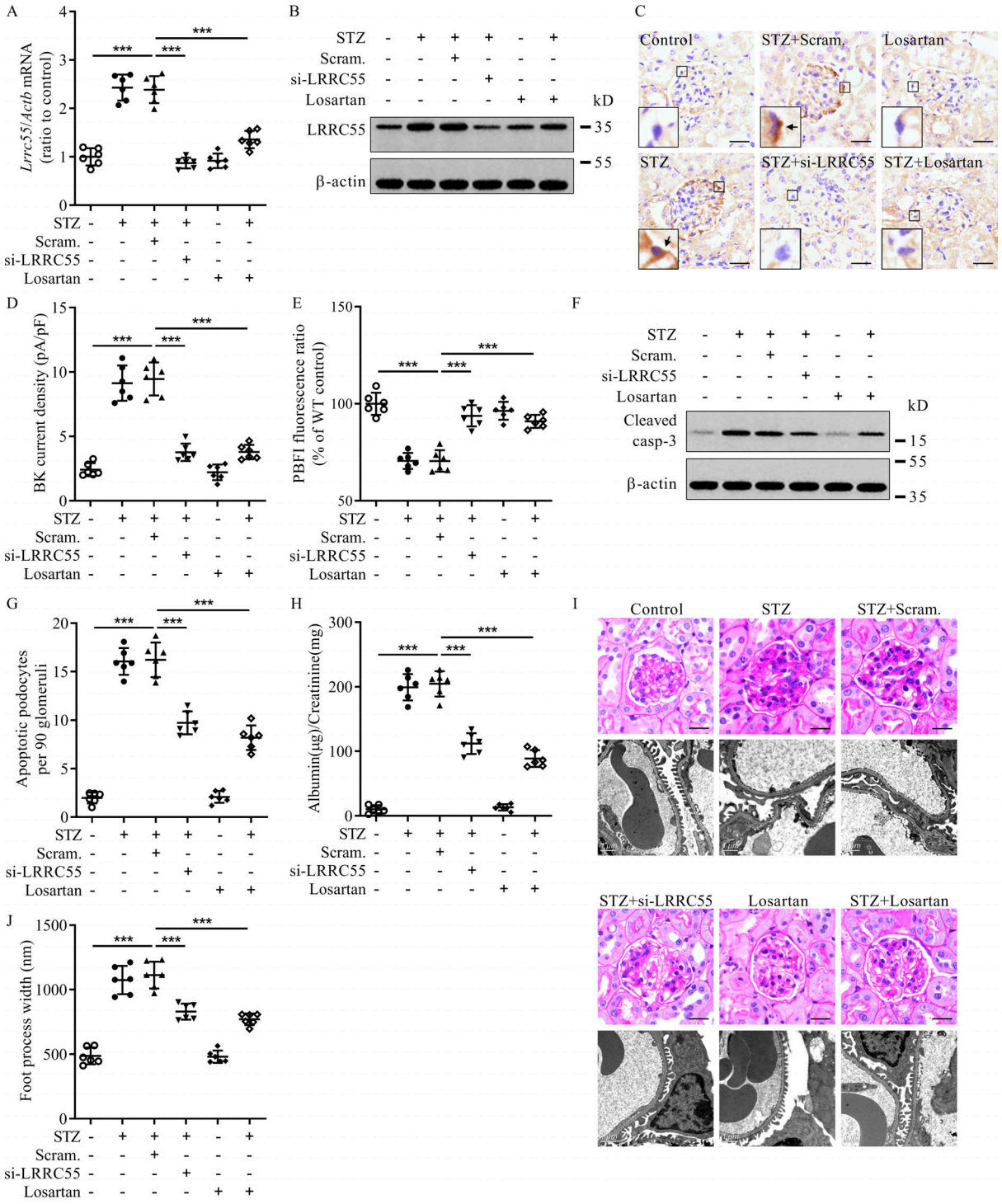

Figure 9. **Effects of losartan on LRRC55 expression and podocyte injury in experimental DN. (A)** The level of *Lrrc55* mRNA in podocytes of diabetic mice treated with losartan or LRRC55 siRNA (n = 6). **(B)** Western blot analysis of LRRC55 expression in podocytes of diabetic mice (n = 6). **(C)** IHC analysis of LRRC55 expression in renal tissues (n = 6). Black arrows indicate positive staining for LRRC55. **(D)** The BK current measured at +80 mV in podocytes of freshly isolated glomeruli from diabetic mice treated with losartan or LRRC55 siRNA (n = 6). **(E)** Intracellular potassium levels in podocytes of freshly isolated glomeruli from diabetic mice treated with losartan or LRRC55 siRNA (n = 6). **(F)** Western blot analysis of cleaved caspase-3 (casp-3) in glomerular tissues of diabetic mice (n = 6). **(G)** The number of apoptotic podocytes in glomerular tissues of diabetic mice (n = 6). **(H)** Urinary albumin excretion of diabetic mice (n = 6). **(I)** Periodic acid–Schiff staining and electron microscopy analysis of renal sections. **(J)** Mean width of podocyte foot processes (n = 6). Data shown are representative of three experiments. For statistical analysis, one-way ANOVA with Tukey's post hoc test was used for A, D, E, G, H, and J. ***, P < 0.001. Scale bar = 20 μm, unless otherwise indicated. Scram., scrambled.

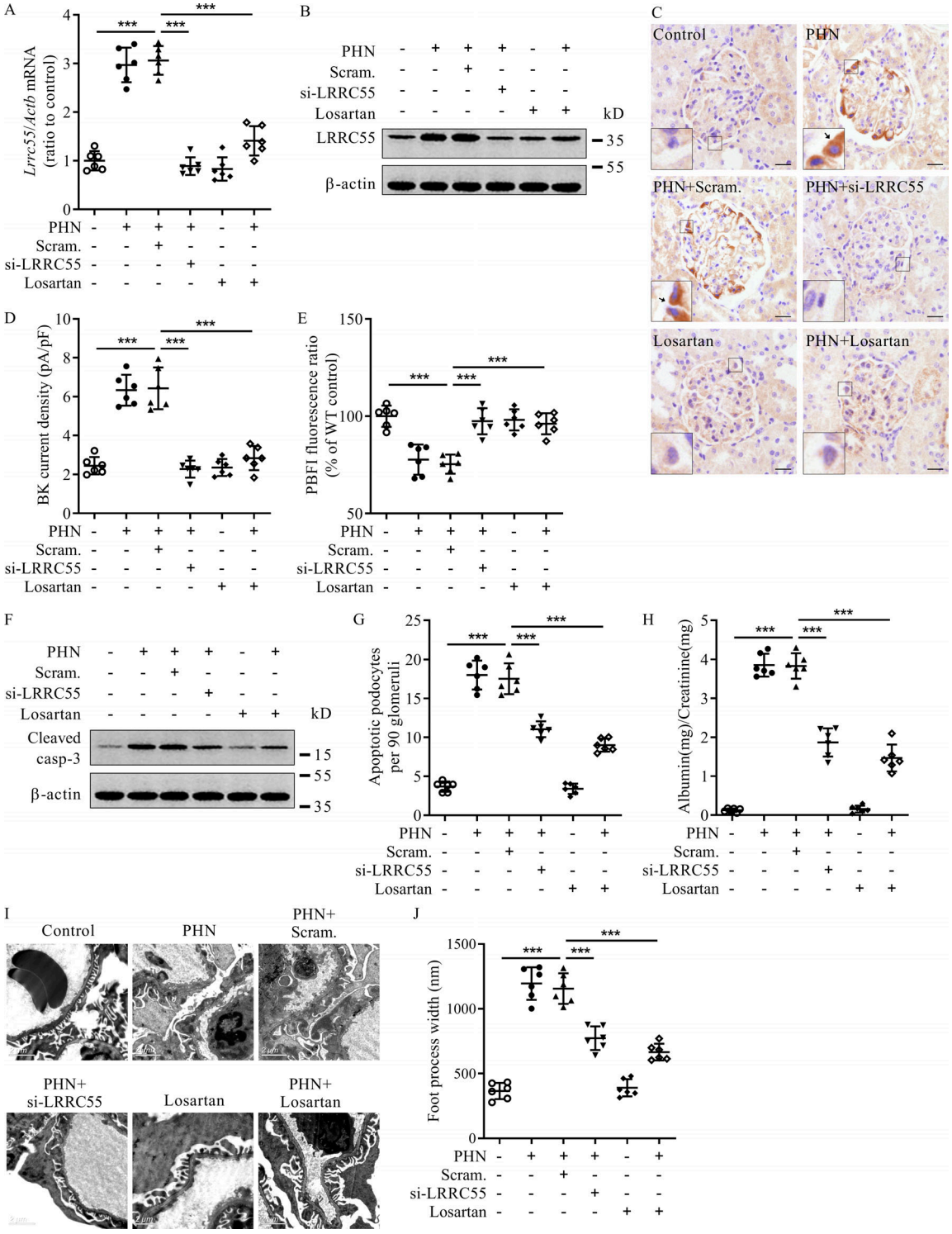

Figure 10. **Effects of losartan on LRRC55 expression and podocyte injury in experimental MN. (A)** The level of *Lrrc55* mRNA in podocytes of PHN rats treated with losartan or LRRC55 siRNA (n = 6). **(B)** Western blot analysis of LRRC55 expression in podocytes of PHN rats (n = 6). **(C)** IHC analysis of LRRC55 expression in renal tissues (n = 6). Black arrows indicate positive staining of LRRC55. **(D)** The BK current measured at +80 mV in podocytes of freshly isolated glomeruli from PHN rats treated with losartan or LRRC55 siRNA (n = 6). **(E)** Intracellular potassium level in podocytes of freshly isolated glomeruli from PHN rats treated with losartan or LRRC55 siRNA (n = 6). **(F)** Western blot analysis of cleaved caspase-3 (casp-3) in glomerular tissues of PHN rats (n = 6). **(G)** The number of apoptotic podocytes in glomerular tissues of PHN rats (n = 6). **(H)** Urinary albumin excretion of PHN rats (n = 6). **(I)** Electron microscopy analysis of renal sections. **(J)** Mean width of podocyte foot processes (n = 6). Data shown are representative of three experiments. For statistical analysis, one-way ANOVA with Tukey's post hoc test was used for A, D, E, G, H, and J. ***, $P < 0.001$. Scale bar = 20 µm, unless otherwise indicated. Scram., scrambled.

the presence of increased intracellular Ca^{2+} (Yan and Aldrich, 2012).

The gating of the BK channel is voltage dependent, and Ca^{2+} binding to multiple allosterically interacting domains in the cytoplasmic C terminus of KCNMA1 proteins shifts the activation into the physiologic range of membrane potentials (Dryer and Reiser, 2010). KCNMA1 binds to the TRPC6 channel in podocytes (Kim et al., 2009). TRPC6 is a slit diaphragm–associated protein involved in the regulation of the filtration function of glomeruli. Sustained activation of TRPC6 signaling leads to podocyte detachment from the glomerular basement membrane due to changes in the cytoskeletal dynamics of foot processes (Winn et al., 2005). Opening of the TRPC6 channel is responsible for Ang II–evoked Ca^{2+} influx in podocytes (Ilatovskaya et al., 2017). We confirmed that treatment with Ang II induced intracellular Ca^{2+} accumulation in podocytes. The BK channel was activated after Ca^{2+} influx, and Ca^{2+} influx was required for Ang II–induced BK channel activation in podocytes. Consistently, Yin et al. (2018) reported that the decrease of Ca^{2+} source resulted in the inhibition of BK currents in podocytes. In addition, the activation of BK channels opposes the cell depolarization caused by TRPC6 activation, thereby maintaining the conditions needed for efficient Ca^{2+} influx (Dryer and Reiser, 2010; Estacion et al., 2006). We observed that activation of the BK channel aggravated TRPC6-mediated Ca^{2+} influx in podocytes.

After TRPC6 activation and Ca^{2+} influx, Ca^{2+} binds to calcineurin and activates its phosphatase activity in podocytes. Activated calcineurin dephosphorylates cytoplasmic NFAT family members, resulting in their translocation to the nucleus where they function as TFs to regulate gene expression (Wu et al., 2015). As shown in a study conducted by Wang et al. (2010), mice displaying NFAT activation in nascent podocytes in utero develop proteinuria and glomerulosclerosis postnatally, reflecting a phenotype resembling FSGS. Among the NFAT family members, NFATc3 is predominantly expressed in podocytes and plays a key role in podocyte injury (Schlöndorff et al., 2009; Wu et al., 2015). Layne et al. (2008) showed that urinary bladder smooth muscle myocytes from *Nfatc3*-null mice displayed a reduced BK channel density compared with myocytes from WT mice. We explored and confirmed that nuclear NFATc3 bound to the promoter region of *LRRC55*, which increased the transcription of *LRRC55*. Treatment with the NFAT-specific inhibitor, 11R-VIVIT, prevented the upregulation of LRRC55 and the activation of BK channels in podocytes from Ang II–treated mice.

Physiologic concentrations of potassium are important for maintaining normal cell functions and inhibiting caspase activation by abrogating Apaf-1 oligomerization (Cain et al., 2001; Ledbetter and Lubin, 1977). Physical and fluorescence techniques have been used to document obvious decreases in intracellular potassium concentrations in apoptotic cells (Hughes and Cidlowski, 1999). In thymocytes and T-cell hybridomas, exposure of isolated nuclei to supernatants of mitochondria that have undergone a permeability transition results in DNA fragmentation if the concentration of the potassium solution is reduced below the physiologic level (Dallaporta et al., 1998). Ang II treatment decreased intracellular potassium in podocytes, and the decreased potassium caused apoptosome formation, caspase-3 activation, and DNA fragmentation in the podocytes. Inhibition of LRRC55 prevented apoptosome formation, caspase-3 activation, and cell apoptosis in podocytes treated with Ang II.

Previously, studies showed that the BK channel was activated in renal mesangial cells and myocytes treated with Ang II (Romero et al., 1998; Sansom et al., 2000; Stockand et al., 1998). We found that the BK channel was activated in Ang II–treated podocytes and podocytes of Ang II–treated mice. Knockout of *Lrrc55* or the BK channel ameliorated podocyte injury in Ang II–treated mice. Abnormal activation of the renin–angiotensin system has been observed in renal tissues of patients with FSGS, DN, and MN (Bahiense-Oliveira et al., 2010; Batlle et al., 2012; Mezzano et al., 2003; Nijenhuis et al., 2011), and increasing evidence indicates that overactivity of the renin–angiotensin system is involved in the progression of glomerular diseases (Rüster and Wolf, 2006). In addition to hemodynamic disorder, activation of the renin–angiotensin system caused renal damage by changing renal protein expression (Koppe and Fouque, 2019; Nijenhuis et al., 2011). Treatment with losartan suppressed LRRC55 expression and prevented BK channel activation in animal models of FSGS, DN, and MN. Angiotensin receptor blockers are one class of antihypertensive drugs that act on the renin–angiotensin system. Beneficial effects of angiotensin receptor blockers on renal outcomes and survival have been observed in patients with various glomerular diseases (Johnson and Spurney, 2015; Sharma et al., 2011). The results are also in line with those of a previous report showing that losartan treatment suppressed Ang II–induced NFAT activation in podocytes (Nijenhuis et al., 2011).

In conclusion, nuclear-translocated NFATc3 induces the expression of LRRC55 in Ang II–exposed podocytes, and upregulated LRRC55 promotes BK channel activation and aggravates cell injury in podocytes in FSGS, DN, and MN. Inhibition of LRRC55 may represent a new therapeutic approach for patients with progressive glomerular diseases.

Materials and methods

Patients and control subjects

Five FSGS patients were recruited for glomerular transcriptome analysis. Another 15 FSGS patients, 15 DN patients, and 15 MN patients were enrolled for the confirmation study (Table S1). Control tissues were obtained from the unaffected portions of surgical nephrectomies and were confirmed to be normal with light microscopy analysis. Samples were kept in the Renal Biobank of National Clinical Research Center of Kidney Diseases, Jiangsu Biobank of Clinical Resources. The study was performed in accordance with the principles of the Declaration of Helsinki and was approved by the ethics committees of Jinling Hospital.

Glomerulus isolation

For array analysis, pink spherical glomeruli were manually isolated under a stereomicroscope using two dissection needle holders in RNAlater at 4°C. The RNA quality and quantity were determined by using the Laboratory-on-Chip Total RNA PicoKit (BioAnalyzer; Agilent Technologies). For PCR analysis, glomeruli were isolated with a laser capture microdissection system (Leica

Microsystems AG). Approximately 50 glomerular cross sections were captured from each case (Bao et al., 2014).

Gene expression profile analysis

Affymetrix HTA2.0 microarrays (Affymetrix) were used to identify differentially expressed genes in microdissected glomerular tissues. Microarray data were deposited in the Gene Expression Omnibus database under accession no. GSE121233.

RT-PCR analysis

Total RNA was extracted by using the Recover All Total Nucleic Acid Isolation Kit (AM1975; Ambion). RT was performed with the RT^2 First Strand Kit (no. 330401; Qiagen). The primers for PCR analysis are listed in Table S2.

IHC and immunofluorescence staining

Paraffin-embedded sections were deparaffinized and rehydrated. Endogenous peroxidase was blocked with 0.3% hydrogen peroxide for 30 min. The sections were incubated for 1 h with anti-LRRC55 antibody diluted in 1% BSA in PBS (Table S3). Staining was visualized with the Polyvalent HRP/DAB detection kit (ab64264; Abcam). Negative controls were obtained by omission of the primary antibody from the staining procedure. The mean density (integrated OD sum/area) of LRRC55 was determined by using the Image 6 Pro Plus system (Media Cybernetics; Dusso et al., 2001; Sun et al., 2012). For immunofluorescence staining, frozen tissue sections were blocked with 1% BSA and incubated in primary antibodies. The sections were then incubated with an FITC-conjugated antibody or a Cy3-conjugated antibody. The slides were examined with a Leica microscope (DM5000B).

Animals

Animal studies were approved by the Institutional Animal Care and Use Committee of Jinling Hospital. *Lrrc55* knockout mice (T037725) and *Kcnma1* knockout mice (T002842) were purchased from the Model Animal Research Center of Nanjing University. For Ang II infusion mouse models, knockout mice and control C57BL/6 mice aged 10–12 wk were randomly assigned to receive Ang II (1,000 ng/kg/min; A9525; Sigma-Aldrich) or saline via implanted subdermal osmotic pumps (Alzet model 2004; Alza Corporation) for 4 wk (Zhao et al., 2017). For the interference study, 11R-VIVIT (1 mg/kg; 480401; Merck) was injected intraperitoneally once per day (Zhang et al., 2013).

As C57BL/6 mice are resistant to ADR-induced nephropathy (Lee and Harris, 2011), ADR nephropathy was induced by injection of 10.5 mg/kg ADR (D1515; Sigma-Aldrich) via the tail vein in BALB/c male mice at age 10–12 wk (Han et al., 2019), and mice were sacrificed at 4 wk after injection. DN was induced in C57BL/6 male mice aged 8 wk by intraperitoneal injection with streptozotocin (STZ; 50 µg/g; S0130; Sigma-Aldrich) for 5 d consecutively. Diabetes was confirmed with a fasting blood glucose level >300 mg/dl. Mice were sacrificed at 12 wk after STZ injection (Fu et al., 2018). The PHN model of MN was induced in male Sprague-Dawley rats aged 7 wk by a single intravenous injection (0.4 ml/100 g) of anti-Fx1A serum (PTX-002S; Probetex; Möller et al., 2007; Sun et al., 2017; Zoja et al., 2002). Control and PHN rats were killed at 28 d after injection. For the interference study, losartan was given by oral gavage at a dose of 10 mg/kg/d for mice (Zhang et al., 2017) and 30 mg/kg/d for rats (Li et al., 2017). LRRC55 siRNA or scrambled siRNA—10 nmol for mice and 20 nmol for rats—was injected via the tail vein with TransIT-QR Delivery Solution (MIR 5210; Minus) before the delivery of ADR, STZ, or anti-Fx1A serum, followed by treatment once per week (Covington and Schnellmann, 2012; Kanai et al., 2009; Lin et al., 2017; Okamoto et al., 2011). Urine was collected in metabolic cages, and albumin and creatinine levels were measured by using Albuwell M (1011; Exocell) and Creatinine Companion Kits (1012; Exocell).

Western blot analysis

Western blots were performed as previously described (Table S3; Bao et al., 2012). Total protein extracts were boiled for 5 min at 95°C, separated by SDS-PAGE, and transferred to polyvinylidene fluoride membranes by using a Bio-Rad transfer unit. The membranes were blocked with 5% nonfat milk diluted in Tris-buffered saline containing 0.1% Tween-20 and incubated with the indicated antibodies. Immunoprecipitation was performed with the Pierce Classic Magnetic IP/Co-IP Kit (88804; Thermo Fisher Scientific).

Electron microscopy and quantification of foot process effacement

Renal cortex tissues were cut into 1-mm^3 pieces, immediately fixed in 3.75% glutaraldehyde and post-fixed in phosphate buffered 1% osmium tetroxide. After dehydration, the specimens were embedded in epoxy resin. Ultrathin sections (70 nm) were stained and examined with a Hitachi 7500 transmission electron microscope. The podocyte foot process effacement was quantified as previously reported (Zhou et al., 2011).

Analysis of podocyte apoptosis in renal tissue

Apoptotic cells were detected by using an in situ terminal deoxynucleotidyl transferase dUTP nick-end labeling (TUNEL) assay (11684795910; Roche Molecular Biochemicals). Tissue sections were costained with DAPI (blue), Wilms tumor 1 antibody (red), and TUNEL (green). Cells labeled by DAPI, Wilms tumor 1, and TUNEL were counted as apoptotic podocytes.

Isolation of rodent glomeruli and podocytes

Mouse glomeruli were isolated by using the magnetic bead–based isolation technique as previously described (Ilatovskaya et al., 2014, 2017; Li et al., 2016). Briefly, mice were anesthetized and perfused with bead solution. The kidneys were then removed, minced into 1-mm^3 pieces, and digested in digestion solution buffer (300 U/ml collagenase type II, 1 mg/ml proteinase E, and 50 U/ml DNase I) for 15 min at 37°C. After digestion, tissues were pressed gently through a 100-µm strainer and collected by centrifugation. The glomeruli were washed three times and collected with a magnet. The isolation of rat glomeruli was similar to the isolation of mouse glomeruli. The tissues were additionally rinsed on a 70-µm cell strainer after collection by a magnet to remove small tubular fragments. The cell strainer was washed and the glomeruli on the cell strainer

were carefully collected (Katsuya et al., 2006). The isolated glomeruli were used for the in situ electrophysiology and intracellular potassium assay in rodent podocytes.

To analyze mRNA and protein levels of LRRC55 in rodent podocytes, part of the separated glomeruli were further digested with 0.025% trypsin or collagenase type IV solution for 10 min at 37°C to obtain single-cell suspensions (Kreisberg et al., 1978; Zhao et al., 2014). After digestion, ice-cold PBS was added to the cell suspension, followed by filtering sequentially through 70-µm and 40-µm cell strainers. The filtered cell suspensions were then centrifuged at 300 ×*g* for 2 min at 4°C. The pellet was resuspended in isolation buffer (prepared in PBS containing 0.1% BSA and 2 mM EDTA). Podocytes were enriched by using anti-podocalyxin beads (Dynabeads FlowComp Flexi; Invitrogen). The viability of the isolated podocytes was >90% according to the trypan blue staining results.

Electrophysiology

Whole-cell recordings were performed in cultured human immortalized podocytes or in rodent podocytes of glomeruli in situ at room temperature (25°C) as previously described (Gloy et al., 1997; Ilatovskaya et al., 2014; Morton et al., 2004). Coverslips with cultured human podocytes or with attached rodent glomeruli were placed into the perfusion chamber and perfused with the bath solution. For BK channel recordings, bath solution contained 145 mM NaCl, 4.5 mM KCl, 1.0 mM $MgCl_2$, 2.0 mM $CaCl_2$, and 10 mM HEPES at pH 7.4. The pipette solutions contained 130 mM K gluconate, 15 mM KCl, 5.76 mM $CaCl_2$ (free Ca^{2+} concentration 200 nM), 1.0 mM $MgCl_2$, 10 mM EGTA, and 10 mM HEPES at pH 7.2. Amphotericin B (0.3 mg/ml; V900919; Sigma-Aldrich) was employed as the permeabilizing agent (Macianskiene et al., 2010). Whole-cell current was evoked by a series of 450-ms depolarizing steps (from −80 to +80 mV in 20-mV increments; Kim et al., 2008, 2010; Morton et al., 2004). For analysis of the TRPC6 current, the bath solution contained 150 mM NaCl, 5.4 mM CsCl, 0.8 mM $MgCl_2$, 5.4 mM $CaCl_2$, and 10 mM HEPES at pH 7.4. The pipette solutions contained 10 mM NaCl, 125 mM CsCl, 6.2 mM $MgCl_2$, 10 mM HEPES, and 10 mM EGTA at pH 7.2. The TRPC6 current was periodically evoked by 2.5-s ramp voltage commands (−80 mV to +80 mV; Kim et al., 2012; Roshanravan et al., 2016). The recording electrodes had resistances of 3–4 MΩ. Currents were amplified (Axopatch 200B), low-pass filtered at 2 kHz, and recorded online at a sampling rate of 4 kHz via a Digidata 1322A interface (Axon Instruments). Data acquisition and analysis was performed with pClamp software (Axon Instruments). The currents were measured at +80 mV and normalized by membrane capacitance.

Podocyte culture and treatment

Immortalized temperature-sensitive human podocytes were provided by M. Saleem (University of Bristol, Bristol, UK), and cells were propagated at a permissive temperature (33°C) in RPMI 1640 medium supplemented with 10% FBS and insulin–transferrin–selenium. The cells were then allowed to differentiate for 2 wk under nonpermissive conditions at 37°C in the same medium (Saleem et al., 2002). The cells were treated with Ang II (1 µM), IBTX (100 nM; I5904; Sigma-Aldrich), or NS1619 (30 µM; N170; Sigma-Aldrich) for indicated times. To infect podocytes with the plenti-CMV-LRRC55 plasmid, the lentiviral stock was mixed with polybrene (1 µg/ml), and the solution was added to the podocytes after removing the culture medium. The transfection of the pREP-NFATc3 plasmid (11790; Addgene), LRRC55 siRNA (sc-96743, 15 nM), TRPC6 siRNA (sc-42672), C/EBPβ siRNA (sc-29229), IRF-2 siRNA (sc-35708), NFATc3 siRNA (sc-29413), STAT4 siRNA (sc-36568), PAX5 siRNA (sc-43996), and ERα siRNA (sc-29305) was conducted with Lipofectamine 2000 (11668–019; Invitrogen).

Intracellular Ca^{2+} assay

For the Ca^{2+} influx assay, cells were incubated in the Ca^{2+} indicator Fluo-4 AM (2 µM; F14217; Thermo Fisher Scientific) for 30 min, and then 1 µM Ang II was added to the cells. Fluorescence images were captured every 5 s. Changes in the intracellular Ca^{2+} level were estimated from the fluorescence images as described previously (Ilatovskaya et al., 2015a).

Intracellular potassium assay

After treatment, cultured human podocytes were loaded with 10 µM PBFI-AM (76275; Sigma-Aldrich) and 0.04% Pluronic F-127 (P2443; Sigma-Aldrich) for 40 min. The ratio of fluorescence intensities obtained by exciting at 340/380 nm while monitoring emissions at 500 nm was used to estimate the intracellular content of potassium (Andersson et al., 2006; Kasner and Ganz, 1992). The intracellular potassium assay in the rodent podocytes of isolated glomeruli in situ was performed as previously described (Ilatovskaya et al., 2014, 2015b). Isolated glomeruli were incubated with 10 µM PBFI-AM, 0.04% Pluronic F-127, and PE-conjugated podocalyxin antibody (1:200; FAB1556P; R&D Systems) for 40 min at room temperature. Glomeruli were then attached to poly-L-lysine–coated glass coverslips. Fluorescence images were acquired by using a Zeiss LSM710 confocal microscope. The mean fluorescence intensities in the podocalyxin-positive cells were analyzed to determine the intracellular potassium level in podocytes of rodent glomeruli (Fig. S5).

DNA fragmentation and caspase-3 activity assay

Cytoplasmic extracts and nuclei were prepared by resuspending the podocytes in 10 mM $MgCl_2$ and 0.25% Nonidet P-40. The nuclei were pelleted and the supernatants were placed on ice. dATP (1 mM) and cytochrome c (10 µg/ml) were added to a mixture of nuclei and cytoplasmic extracts with various concentrations of KCl (Hughes et al., 1997). DNA was extracted and analyzed with 1.5% agarose gel electrophoresis. The caspase-3 protease activity was measured with Z-DEVD-AFC (sc-296746; Santa Cruz Biotechnology) as the fluorogenic substrate.

Apoptosis analysis with flow cytometry

The detection of apoptotic podocytes was performed by using the FITC Annexin Apoptosis Detection Kit I (556547; BD Biosciences).

Promoter-binding TF profiling plate array

Promoter-binding TF profiling plate array analysis (FA-2001; Signosis) was performed according to the manufacturer's

instruction. Podocytes were treated with Ang II for 24 h to activate TFs. Nuclear extracts were prepared and incubated with TF binding oligo probe mix with or without the *LRRC55* promoter fragment. After spin separation of the complexes from unbound free biotin-labeled oligos, TF-bound probes were eluted from the column and used for plate hybridization. The captured probes were detected with streptavidin-HRP and chemiluminescent substrate.

ChIP analysis of NFATc3 DNA binding

The ChIP assay was performed with the ChIP-IT Express Magnetic Chromatin Immunoprecipitation Kit (53008; Active Motif) and anti-NFATc3 or IgG antibodies (Bao et al., 2014).

Luciferase assays

Cells were cotransfected with the 0.1 µg reporter constructs, 0.02 µg *Renilla* construct, and 0.1 µg pREP-NFATc3 plasmid. The firefly and *Renilla* luciferase activity were determined by using the Dual-Luciferase Reporter Assay System (E1960; Promega). The values were normalized with *Renilla* luciferase (Bao et al., 2014).

Statistical analysis

All of the data are expressed as mean ± SD. Data from multiple groups were analyzed via one-way ANOVA followed by Tukey's post hoc test. Data from two groups were compared using *t* tests. Results with a P value of <0.05 were considered significant: *, $P < 0.05$; **, $P < 0.01$; and ***, $P < 0.001$.

Online supplemental material

Fig. S1 shows the level of LRRC55 in glomerular tissues of patients with interstitial nephritis or MCD. Fig. S2 is a schematic diagram of the whole-cell recordings of the BK current in rodent podocytes of glomeruli in situ. Fig. S3 displays the Western blot analysis of LRRC55 or TRPC6 in podocytes. Fig. S4 shows that the activation of the BK channel exacerbates TRPC6-mediated Ca^{2+} influx in podocytes. Fig. S5 depicts the intracellular potassium assay in the podocytes of isolated rodent glomeruli in situ. Table S1 provides the clinical and pathologic characteristics of the discovery and validation cohorts. Table S2 lists the primers used in this study. Table S3 lists the antibodies used in this study.

Acknowledgments

We thank the physicians, patients, and volunteers who contributed to this study.

This work is supported by grants from the National Natural Science Foundation of China (81873610 and 81200516 to H. Bao), the Natural Science Foundation of Jiangsu Province (BK20171330 and BK2012372), the Deng Feng Scholars of Nanjing University (to H. Bao), the Fundamental Research Funds for the Central Universities (to H. Bao), the National Natural Science Foundation of China (81770701 and 81600560 to X. Xu), the National Key Research and Development Program of China (2016YFC0904103), and the Major International (Regional) Joint Research Programme (81320108007).

Author contributions: H. Bao and Z. Liu designed the study; S. Hu, L. Chen, R. Han, W. Qin, X. Xu, X. Zhu, M. Zhang, C. Zeng, and Z. Tang performed the experiments; J. Shi performed data bioinformatics analysis; and H. Bao and S. Hu wrote the manuscript.

Disclosures: The authors declare no competing interests exist.

Submitted: 19 December 2019
Revised: 27 July 2020
Accepted: 16 September 2020

References

Andersson, B., V. Janson, P. Behnam-Motlagh, R. Henriksson, and K. Grankvist. 2006. Induction of apoptosis by intracellular potassium ion depletion: using the fluorescent dye PBFI in a 96-well plate method in cultured lung cancer cells. *Toxicol. In Vitro.* 20:986–994. https://doi.org/10.1016/j.tiv.2005.12.013

Bahiense-Oliveira, M., A.L. Mattar, D.M. Malheiros, and V. Woronik. 2010. Interstitial expression of angiotensin II and AT1 receptor are increased in patients with progressive glomerulopathies. *J. Renin Angiotensin Aldosterone Syst.* 11:158–164. https://doi.org/10.1177/1470320310367929

Bao, H., Y. Ge, S. Zhuang, L.D. Dworkin, Z. Liu, and R. Gong. 2012. Inhibition of glycogen synthase kinase-3β prevents NSAID-induced acute kidney injury. *Kidney Int.* 81:662–673. https://doi.org/10.1038/ki.2011.443

Bao, H., H. Chen, X. Zhu, M. Zhang, G. Yao, Y. Yu, W. Qin, C. Zeng, K. Zen, and Z. Liu. 2014. MiR-223 downregulation promotes glomerular endothelial cell activation by upregulating importin α4 and α5 in IgA nephropathy. *Kidney Int.* 85:624–635. https://doi.org/10.1038/ki.2013.469

Batlle, D., J. Wysocki, M.J. Soler, and K. Ranganath. 2012. Angiotensin-converting enzyme 2: enhancing the degradation of angiotensin II as a potential therapy for diabetic nephropathy. *Kidney Int.* 81:520–528. https://doi.org/10.1038/ki.2011.381

Burg, E.D., C.V. Remillard, and J.X. Yuan. 2006. K+ channels in apoptosis. *J. Membr. Biol.* 209:3–20. https://doi.org/10.1007/s00232-005-0838-4

Cain, K., C. Langlais, X.M. Sun, D.G. Brown, and G.M. Cohen. 2001. Physiological concentrations of K+ inhibit cytochrome c-dependent formation of the apoptosome. *J. Biol. Chem.* 276:41985–41990. https://doi.org/10.1074/jbc.M107419200

Covington, M.D., and R.G. Schnellmann. 2012. Chronic high glucose downregulates mitochondrial calpain 10 and contributes to renal cell death and diabetes-induced renal injury. *Kidney Int.* 81:391–400. https://doi.org/10.1038/ki.2011.356

Dallaporta, B., T. Hirsch, S.A. Susin, N. Zamzami, N. Larochette, C. Brenner, I. Marzo, and G. Kroemer. 1998. Potassium leakage during the apoptotic degradation phase. *J. Immunol.* 160:5605–5615.

Dryer, S.E., and J. Reiser. 2010. TRPC6 channels and their binding partners in podocytes: role in glomerular filtration and pathophysiology. *Am. J. Physiol. Renal Physiol.* 299:F689–F701. https://doi.org/10.1152/ajprenal.00298.2010

Dusso, A.S., T. Pavlopoulos, L. Naumovich, Y. Lu, J. Finch, A.J. Brown, J. Morrissey, and E. Slatopolsky. 2001. p21(WAF1) and transforming growth factor-alpha mediate dietary phosphate regulation of parathyroid cell growth. *Kidney Int.* 59:855–865. https://doi.org/10.1046/j.1523-1755.2001.059003855.x

Estacion, M., W.G. Sinkins, S.W. Jones, M.A. Applegate, and W.P. Schilling. 2006. Human TRPC6 expressed in HEK 293 cells forms non-selective cation channels with limited Ca2+ permeability. *J. Physiol.* 572:359–377. https://doi.org/10.1113/jphysiol.2005.103143

Fu, J., C. Wei, W. Zhang, D. Schlondorff, J. Wu, M. Cai, W. He, M.H. Baron, P.Y. Chuang, Z. Liu, et al. 2018. Gene expression profiles of glomerular endothelial cells support their role in the glomerulopathy of diabetic mice. *Kidney Int.* 94:326–345. https://doi.org/10.1016/j.kint.2018.02.028

Gloy, J., A. Henger, K.G. Fischer, R. Nitschke, P. Mundel, M. Bleich, P. Schollmeyer, R. Greger, and H. Pavenstädt. 1997. Angiotensin II depolarizes podocytes in the intact glomerulus of the Rat. *J. Clin. Invest.* 99:2772–2781. https://doi.org/10.1172/JCI119467

Han, R., S. Hu, W. Qin, J. Shi, Q. Hou, X. Wang, X. Xu, M. Zhang, C. Zeng, Z. Liu, et al. 2019. C3a and suPAR drive versican V1 expression in tubular cells of focal segmental glomerulosclerosis. *JCI Insight.* 4:e122912. https://doi.org/10.1172/jci.insight.122912

Hanamura, K., A. Tojo, and T. Fujita. 2014. Urinary and glomerular podocytes in patients with chronic kidney diseases. *Clin. Exp. Nephrol.* 18:95–103. https://doi.org/10.1007/s10157-013-0814-8

Hughes, F.M. Jr., and J.A. Cidlowski. 1999. Potassium is a critical regulator of apoptotic enzymes in vitro and in vivo. *Adv. Enzyme Regul.* 39:157–171. https://doi.org/10.1016/S0065-2571(98)00010-7

Hughes, F.M. Jr., C.D. Bortner, G.D. Purdy, and J.A. Cidlowski. 1997. Intracellular K+ suppresses the activation of apoptosis in lymphocytes. *J. Biol. Chem.* 272:30567–30576. https://doi.org/10.1074/jbc.272.48.30567

Ilatovskaya, D.V., and A. Staruschenko. 2015. TRPC6 channel as an emerging determinant of the podocyte injury susceptibility in kidney diseases. *Am. J. Physiol. Renal Physiol.* 309:F393–F397. https://doi.org/10.1152/ajprenal.00186.2015

Ilatovskaya, D.V., O. Palygin, V. Chubinskiy-Nadezhdin, Y.A. Negulyaev, R. Ma, L. Birnbaumer, and A. Staruschenko. 2014. Angiotensin II has acute effects on TRPC6 channels in podocytes of freshly isolated glomeruli. *Kidney Int.* 86:506–514. https://doi.org/10.1038/ki.2014.71

Ilatovskaya, D.V., V. Levchenko, A. Lowing, L.S. Shuyskiy, O. Palygin, and A. Staruschenko. 2015a. Podocyte injury in diabetic nephropathy: implications of angiotensin II-dependent activation of TRPC channels. *Sci. Rep.* 5:17637. https://doi.org/10.1038/srep17637

Ilatovskaya, D.V., O. Palygin, V. Levchenko, and A. Staruschenko. 2015b. Single-channel Analysis and Calcium Imaging in the Podocytes of the Freshly Isolated Glomeruli. *J. Vis. Exp.* 2015:e52850.

Ilatovskaya, D.V., O. Palygin, V. Levchenko, B.T. Endres, and A. Staruschenko. 2017. The role of angiotensin II in glomerular volume dynamics and podocyte calcium handling. *Sci. Rep.* 7:299. https://doi.org/10.1038/s41598-017-00406-2

Johnson, S.A., and R.F. Spurney. 2015. Twenty years after ACEIs and ARBs: emerging treatment strategies for diabetic nephropathy. *Am. J. Physiol. Renal Physiol.* 309:F807–F820. https://doi.org/10.1152/ajprenal.00266.2015

Kanai, G., T. Kakuta, K. Sawada, T.A. Yokoyama, R. Tanaka, and A. Saito. 2009. Suppression of parathyroid hormone production in vitro and in vivo by RNA interference. *Kidney Int.* 75:490–498. https://doi.org/10.1038/ki.2008.568

Kasner, S.E., and M.B. Ganz. 1992. Regulation of intracellular potassium in mesangial cells: a fluorescence analysis using the dye, PBFI. *Am. J. Physiol.* 262:F462–F467.

Katsuya, K., E. Yaoita, Y. Yoshida, Y. Yamamoto, and T. Yamamoto. 2006. An improved method for primary culture of rat podocytes. *Kidney Int.* 69:2101–2106. https://doi.org/10.1038/sj.ki.5000398

Kim, E.Y., K.J. Choi, and S.E. Dryer. 2008. Nephrin binds to the COOH terminus of a large-conductance Ca2+-activated K+ channel isoform and regulates its expression on the cell surface. *Am. J. Physiol. Renal Physiol.* 295:F235–F246. https://doi.org/10.1152/ajprenal.00140.2008

Kim, E.Y., C.P. Alvarez-Baron, and S.E. Dryer. 2009. Canonical transient receptor potential channel (TRPC)3 and TRPC6 associate with large-conductance Ca2+-activated K+ (BKCa) channels: role in BKCa trafficking to the surface of cultured podocytes. *Mol. Pharmacol.* 75:466–477. https://doi.org/10.1124/mol.108.051912

Kim, E.Y., J.M. Suh, Y.H. Chiu, and S.E. Dryer. 2010. Regulation of podocyte BK(Ca) channels by synaptopodin, Rho, and actin microfilaments. *Am. J. Physiol. Renal Physiol.* 299:F594–F604. https://doi.org/10.1152/ajprenal.00206.2010

Kim, E.Y., M. Anderson, and S.E. Dryer. 2012. Insulin increases surface expression of TRPC6 channels in podocytes: role of NADPH oxidases and reactive oxygen species. *Am. J. Physiol. Renal Physiol.* 302:F298–F307. https://doi.org/10.1152/ajprenal.00423.2011

Koppe, L., and D. Fouque. 2019. The role for protein restriction in addition to renin-angiotensin-aldosterone system inhibitors in the management of CKD. *Am. J. Kidney Dis.* 73:248–257. https://doi.org/10.1053/j.ajkd.2018.06.016

Kreisberg, J.I., R.L. Hoover, and M.J. Karnovsky. 1978. Isolation and characterization of rat glomerular epithelial cells in vitro. *Kidney Int.* 14:21–30. https://doi.org/10.1038/ki.1978.86

Krick, S., O. Platoshyn, M. Sweeney, H. Kim, and J.X. Yuan. 2001. Activation of K+ channels induces apoptosis in vascular smooth muscle cells. *Am. J. Physiol. Cell Physiol.* 280:C970–C979. https://doi.org/10.1152/ajpcell.2001.280.4.C970

Layne, J.J., M.E. Werner, D.C. Hill-Eubanks, and M.T. Nelson. 2008. NFATc3 regulates BK channel function in murine urinary bladder smooth muscle. *Am. J. Physiol. Cell Physiol.* 295:C611–C623. https://doi.org/10.1152/ajpcell.00435.2007

Ledbetter, M.L., and M. Lubin. 1977. Control of protein synthesis in human fibroblasts by intracellular potassium. *Exp. Cell Res.* 105:223–236. https://doi.org/10.1016/0014-4827(77)90120-3

Lee, V.W., and D.C. Harris. 2011. Adriamycin nephropathy: a model of focal segmental glomerulosclerosis. *Nephrology (Carlton).* 16:30–38. https://doi.org/10.1111/j.1440-1797.2010.01383.x

Li, Q., F. Fan, H.R. Kwak, and J. Yan. 2015. Molecular basis for differential modulation of BK channel voltage-dependent gating by auxiliary γ subunits. *J. Gen. Physiol.* 145:543–554. https://doi.org/10.1085/jgp.201511356

Li, C., Y. Ge, L. Dworkin, A. Peng, and R. Gong. 2016. The β isoform of GSK3 mediates podocyte autonomous injury in proteinuric glomerulopathy. *J. Pathol.* 239:23–35. https://doi.org/10.1002/path.4692

Li, W.J., M. Xu, M. Gu, D.C. Zheng, J. Guo, Z. Cai, and Z. Wang. 2017. Losartan preserves erectile function by suppression of apoptosis and fibrosis of corpus cavernosum and corporal veno-occlusive dysfunction in diabetic rats. *Cell. Physiol. Biochem.* 42:333–345. https://doi.org/10.1159/000477388

Lin, W., Q. Zhang, L. Liu, S. Yin, Z. Liu, and W. Cao. 2017. Klotho restoration via acetylation of Peroxisome Proliferation-Activated Receptor γ reduces the progression of chronic kidney disease. *Kidney Int.* 92:669–679. https://doi.org/10.1016/j.kint.2017.02.023

Lu, R., A. Alioua, Y. Kumar, M. Eghbali, E. Stefani, and L. Toro. 2006. MaxiK channel partners: physiological impact. *J. Physiol.* 570:65–72. https://doi.org/10.1113/jphysiol.2005.098913

Ma, Y.G., L. Dong, X.L. Ye, C.L. Deng, J.H. Cheng, W.C. Liu, J. Ma, Y.M. Chang, and M.J. Xie. 2010. Activation of cloned BK(Ca) channels in nitric oxide-induced apoptosis of HEK293 cells. *Apoptosis.* 15:426–438. https://doi.org/10.1007/s10495-009-0423-x

Ma, Y.G., W.C. Liu, S. Dong, C. Du, X.J. Wang, J.S. Li, X.P. Xie, L. Wu, D.C. Ma, Z.B. Yu, and M.J. Xie. 2012. Activation of BK(Ca) channels in zoledronic acid-induced apoptosis of MDA-MB-231 breast cancer cells. *PLoS One.* 7:e37451. https://doi.org/10.1371/journal.pone.0037451

Macianskiene, R., A. Gwanyanya, K.R. Sipido, J. Vereecke, and K. Mubagwa. 2010. Induction of a novel cation current in cardiac ventricular myocytes by flufenamic acid and related drugs. *Br. J. Pharmacol.* 161:416–429. https://doi.org/10.1111/j.1476-5381.2010.00901.x

Mezzano, S.A., C.A. Aros, A. Droguett, M.E. Burgos, L.G. Ardiles, C.A. Flores, D. Carpio, C.P. Vío, M. Ruiz-Ortega, and J. Egido. 2003. Renal angiotensin II up-regulation and myofibroblast activation in human membranous nephropathy. *Kidney Int. Suppl.* 64:S39–S45. https://doi.org/10.1046/j.1523-1755.64.s86.8.x

Möller, C.C., C. Wei, M.M. Altintas, J. Li, A. Greka, T. Ohse, J.W. Pippin, M.P. Rastaldi, S. Wawersik, S. Schiavi, et al. 2007. Induction of TRPC6 channel in acquired forms of proteinuric kidney disease. *J. Am. Soc. Nephrol.* 18:29–36. https://doi.org/10.1681/ASN.2006091010

Morton, M.J., K. Hutchinson, P.W. Mathieson, I.R. Witherden, M.A. Saleem, and M. Hunter. 2004. Human podocytes possess a stretch-sensitive, Ca2+-activated K+ channel: potential implications for the control of glomerular filtration. *J. Am. Soc. Nephrol.* 15:2981–2987. https://doi.org/10.1097/01.ASN.0000145046.24268.0D

Nagata, M. 2016. Podocyte injury and its consequences. *Kidney Int.* 89:1221–1230. https://doi.org/10.1016/j.kint.2016.01.012

Nakagawa, S., K. Nishihara, H. Miyata, H. Shinke, E. Tomita, M. Kajiwara, T. Matsubara, N. Iehara, Y. Igarashi, H. Yamada, et al. 2015. Molecular markers of tubulointerstitial fibrosis and tubular cell damage in patients with chronic kidney disease. *PLoS One.* 10:e0136994. https://doi.org/10.1371/journal.pone.0136994

Nakamura, T., C. Ushiyama, S. Suzuki, M. Hara, N. Shimada, I. Ebihara, and H. Koide. 2000. The urinary podocyte as a marker for the differential diagnosis of idiopathic focal glomerulosclerosis and minimal-change nephrotic syndrome. *Am. J. Nephrol.* 20:175–179. https://doi.org/10.1159/000013580

Nijenhuis, T., A.J. Sloan, J.G. Hoenderop, J. Flesche, H. van Goor, A.D. Kistler, M. Bakker, R.J. Bindels, R.A. de Boer, C.C. Möller, et al. 2011. Angiotensin II contributes to podocyte injury by increasing TRPC6 expression via an NFAT-mediated positive feedback signaling pathway. *Am. J. Pathol.* 179:1719–1732. https://doi.org/10.1016/j.ajpath.2011.06.033

Okamoto, K., K. Tokunaga, K. Doi, T. Fujita, H. Suzuki, T. Katoh, T. Watanabe, N. Nishida, A. Mabuchi, A. Takahashi, et al. 2011. Common variation in GPC5 is associated with acquired nephrotic syndrome. *Nat. Genet.* 43:459–463. https://doi.org/10.1038/ng.792

Piwkowska, A., D. Rogacka, I. Audzeyenka, M. Kasztan, S. Angielski, and M. Jankowski. 2015. Insulin increases glomerular filtration barrier permeability through PKGIα-dependent mobilization of BKCa channels in cultured rat podocytes. *Biochim. Biophys. Acta.* 1852:1599–1609. https://doi.org/10.1016/j.bbadis.2015.04.024

Romero, F., B.A. Silva, V.L. Nouailhetas, and J. Aboulafia. 1998. Activation of Ca(2+)-activated K+ (maxi-K+) channel by angiotensin II in myocytes of the guinea pig ileum. *Am. J. Physiol.* 274:C983–C991. https://doi.org/10.1152/ajpcell.1998.274.4.C983

Roshanravan, H., E.Y. Kim, and S.E. Dryer. 2016. 20-Hydroxyeicosatetraenoic acid (20-HETE) modulates canonical transient receptor potential-6 (TRPC6) channels in podocytes. *Front. Physiol.* 7:351. https://doi.org/10.3389/fphys.2016.00351

Rüster, C., and G. Wolf. 2006. Renin-angiotensin-aldosterone system and progression of renal disease. *J. Am. Soc. Nephrol.* 17:2985–2991. https://doi.org/10.1681/ASN.2006040356

Saleem, M.A., M.J. O'Hare, J. Reiser, R.J. Coward, C.D. Inward, T. Farren, C.Y. Xing, L. Ni, P.W. Mathieson, and P. Mundel. 2002. A conditionally immortalized human podocyte cell line demonstrating nephrin and podocin expression. *J. Am. Soc. Nephrol.* 13:630–638.

Sampson, M.G., C.C. Robertson, S. Martini, L.H. Mariani, K.V. Lemley, C.E. Gillies, E.A. Otto, J.B. Kopp, A. Randolph, V. Vega-Warner, et al. Nephrotic Syndrome Study Network. 2016. Integrative genomics identifies novel associations with APOL1 risk genotypes in black NEPTUNE subjects. *J. Am. Soc. Nephrol.* 27:814–823. https://doi.org/10.1681/ASN.2014111131

Sansom, S.C., R. Ma, P.K. Carmines, and D.A. Hall. 2000. Regulation of Ca(2+)-activated K(+) channels by multifunctional Ca(2+)/calmodulin-dependent protein kinase. *Am. J. Physiol. Renal Physiol.* 279:F283–F288. https://doi.org/10.1152/ajprenal.2000.279.2.F283

Schlöndorff, J., D. Del Camino, R. Carrasquillo, V. Lacey, and M.R. Pollak. 2009. TRPC6 mutations associated with focal segmental glomerulosclerosis cause constitutive activation of NFAT-dependent transcription. *Am. J. Physiol. Cell Physiol.* 296:C558–C569. https://doi.org/10.1152/ajpcell.00077.2008

Schreiber, M., and L. Salkoff. 1997. A novel calcium-sensing domain in the BK channel. *Biophys. J.* 73:1355–1363. https://doi.org/10.1016/S0006-3495(97)78168-2

Shankland, S.J. 2006. The podocyte's response to injury: role in proteinuria and glomerulosclerosis. *Kidney Int.* 69:2131–2147. https://doi.org/10.1038/sj.ki.5000410

Sharma, P., R.C. Blackburn, C.L. Parke, K. McCullough, A. Marks, and C. Black. 2011. Angiotensin-converting enzyme inhibitors and angiotensin receptor blockers for adults with early (stage 1 to 3) non-diabetic chronic kidney disease. *Cochrane Database Syst. Rev.* 2011:CD007751.

Stockand, J.D., M. Silverman, D. Hall, T. Derr, B. Kubacak, and S.C. Sansom. 1998. Arachidonic acid potentiates the feedback response of mesangial BKCa channels to angiotensin II. *Am. J. Physiol.* 274:F658–F664.

Sun, D., Y. Wang, C. Liu, X. Zhou, X. Li, and A. Xiao. 2012. Effects of nitric oxide on renal interstitial fibrosis in rats with unilateral ureteral obstruction. *Life Sci.* 90:900–909. https://doi.org/10.1016/j.lfs.2012.04.018

Sun, H., H.S. Olsen, E.Y. Mérigeon, E. So, E. Burch, S. Kinsey, J.C. Papadimitriou, C.B. Drachenberg, S.M. Bentzen, D.S. Block, et al. 2017. Recombinant human IgG1 based Fc multimers, with limited FcR binding capacity, can effectively inhibit complement-mediated disease. *J. Autoimmun.* 84:97–108. https://doi.org/10.1016/j.jaut.2017.08.004

Wang, Y., G. Jarad, P. Tripathi, M. Pan, J. Cunningham, D.R. Martin, H. Liapis, J.H. Miner, and F. Chen. 2010. Activation of NFAT signaling in podocytes causes glomerulosclerosis. *J. Am. Soc. Nephrol.* 21:1657–1666. https://doi.org/10.1681/ASN.2009121253

Wiggins, R.C. 2007. The spectrum of podocytopathies: a unifying view of glomerular diseases. *Kidney Int.* 71:1205–1214. https://doi.org/10.1038/sj.ki.5002222

Winn, M.P., P.J. Conlon, K.L. Lynn, M.K. Farrington, T. Creazzo, A.F. Hawkins, N. Daskalakis, S.Y. Kwan, S. Ebersviller, J.L. Burchette, et al. 2005. A mutation in the TRPC6 cation channel causes familial focal segmental glomerulosclerosis. *Science.* 308:1801–1804. https://doi.org/10.1126/science.1106215

Wu, J., C. Zheng, X. Wang, S. Yun, Y. Zhao, L. Liu, Y. Lu, Y. Ye, X. Zhu, C. Zhang, et al. 2015. MicroRNA-30 family members regulate calcium/calcineurin signaling in podocytes. *J. Clin. Invest.* 125:4091–4106. https://doi.org/10.1172/JCI81061

Xu, L., H.C. Yang, C.M. Hao, S.T. Lin, Y. Gu, and J. Ma. 2010. Podocyte number predicts progression of proteinuria in IgA nephropathy. *Mod. Pathol.* 23:1241–1250. https://doi.org/10.1038/modpathol.2010.110

Yan, J., and R.W. Aldrich. 2010. LRRC26 auxiliary protein allows BK channel activation at resting voltage without calcium. *Nature.* 466:513–516. https://doi.org/10.1038/nature09162

Yan, J., and R.W. Aldrich. 2012. BK potassium channel modulation by leucine-rich repeat-containing proteins. *Proc. Natl. Acad. Sci. USA.* 109:7917–7922. https://doi.org/10.1073/pnas.1205435109

Yin, H., X. Zhang, K. Li, Z. Li, and Z. Yang. 2018. Effects of miR-200b-3p inhibition on the TRPC6 and BK_{Ca} channels of podocytes. *Arch. Biochem. Biophys.* 653:80–89. https://doi.org/10.1016/j.abb.2018.06.013

Zhang, J., and J. Yan. 2014. Regulation of BK channels by auxiliary γ subunits. *Front. Physiol.* 5:401. https://doi.org/10.3389/fphys.2014.00401

Zhang, L., R. Li, W. Shi, X. Liang, S. Liu, Z. Ye, C. Yu, Y. Chen, B. Zhang, W. Wang, et al. 2013. NFAT2 inhibitor ameliorates diabetic nephropathy and podocyte injury in db/db mice. *Br. J. Pharmacol.* 170:426–439. https://doi.org/10.1111/bph.12292

Zhang, M.Z., X. Wang, H. Yang, A.B. Fogo, B.J. Murphy, R. Kaltenbach, P. Cheng, B. Zinker, and R.C. Harris. 2017. Lysophosphatidic acid receptor antagonism protects against diabetic nephropathy in a type 2 diabetic model. *J. Am. Soc. Nephrol.* 28:3300–3311. https://doi.org/10.1681/ASN.2017010107

Zhao, Y., H. Zhao, Y. Zhang, T. Tsatralis, Q. Cao, Y. Wang, Y. Wang, Y.M. Wang, S.I. Alexander, D.C. Harris, and G. Zheng. 2014. Isolation and epithelial co-culture of mouse renal peritubular endothelial cells. *BMC Cell Biol.* 15:40. https://doi.org/10.1186/s12860-014-0040-6

Zhao, Y., J. Wu, M. Zhang, M. Zhou, F. Xu, X. Zhu, X. Zhou, Y. Lang, F. Yang, S. Yun, et al. 2017. Angiotensin II induces calcium/calcineurin signaling and podocyte injury by downregulating microRNA-30 family members. *J. Mol. Med. (Berl.).* 95:887–898. https://doi.org/10.1007/s00109-017-1547-z

Zhou, Y., X. Kong, P. Zhao, H. Yang, L. Chen, J. Miao, X. Zhang, J. Yang, J. Ding, and Y. Guan. 2011. Peroxisome proliferator-activated receptor-α is renoprotective in doxorubicin-induced glomerular injury. *Kidney Int.* 79:1302–1311. https://doi.org/10.1038/ki.2011.17

Zoja, C., D. Corna, D. Camozzi, D. Cattaneo, D. Rottoli, C. Batani, C. Zanchi, M. Abbate, and G. Remuzzi. 2002. How to fully protect the kidney in a severe model of progressive nephropathy: a multidrug approach. *J. Am. Soc. Nephrol.* 13:2898–2908. https://doi.org/10.1097/01.ASN.0000034912.55186.EC

Supplemental material

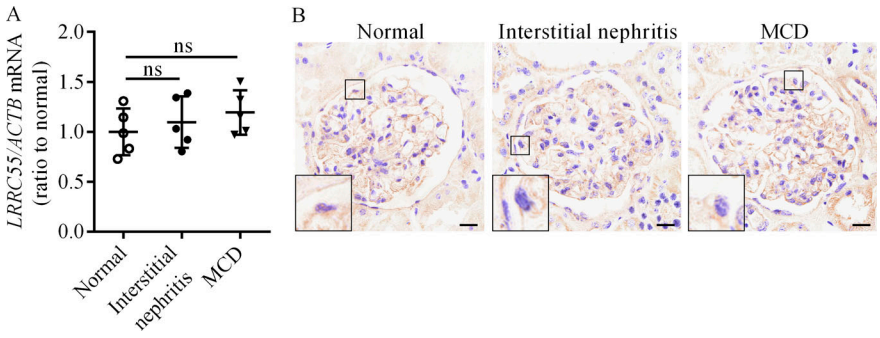

Figure S1. **The level of LRRC55 in glomerular tissues of patients with interstitial nephritis or MCD. (A)** RT-PCR analysis of *LRRC55* in glomerular tissues of patients with interstitial nephritis or MCD (n = 5). **(B)** IHC analysis of LRRC55 expression in renal tissues of patients with interstitial nephritis or MCD (n = 5). Data shown are representative of three experiments. For statistical analysis, one-way ANOVA with Tukey's post hoc test was used for A. ns, not significant. Scale bar = 20 µm.

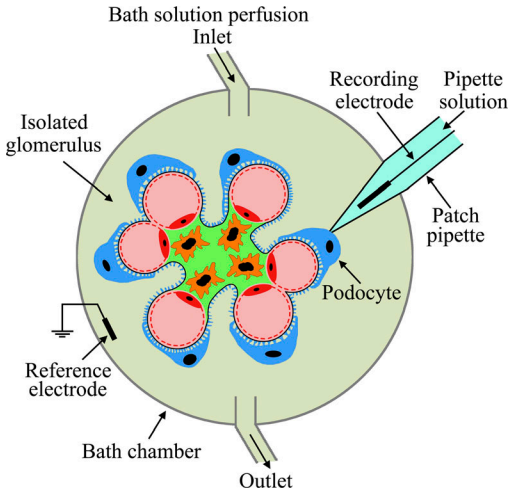

Figure S2. **Schematic diagram of the whole-cell recordings of the BK current in rodent podocytes of glomeruli in situ**. Isolated rodent glomeruli were attached to poly-L-lysine–coated coverslips, and then the coverslips were placed into a patch-clamp chamber and perfused with bath solution to conduct a patch-clamp experiment.

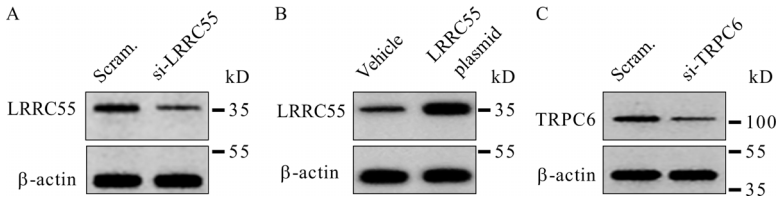

Figure S3. **Western blot analysis of LRRC55 or TRPC6 in podocytes. (A)** Level of LRRC55 in podocytes transfected with LRRC55 siRNA for 24 h (n = 3). **(B)** Level of LRRC55 in podocytes transfected with LRRC55 expression plasmid for 24 h (n = 3). **(C)** Level of TRPC6 in podocytes transfected with TRPC6 siRNA for 24 h (n = 3). Results are representative of three experiments. Scram., scrambled.

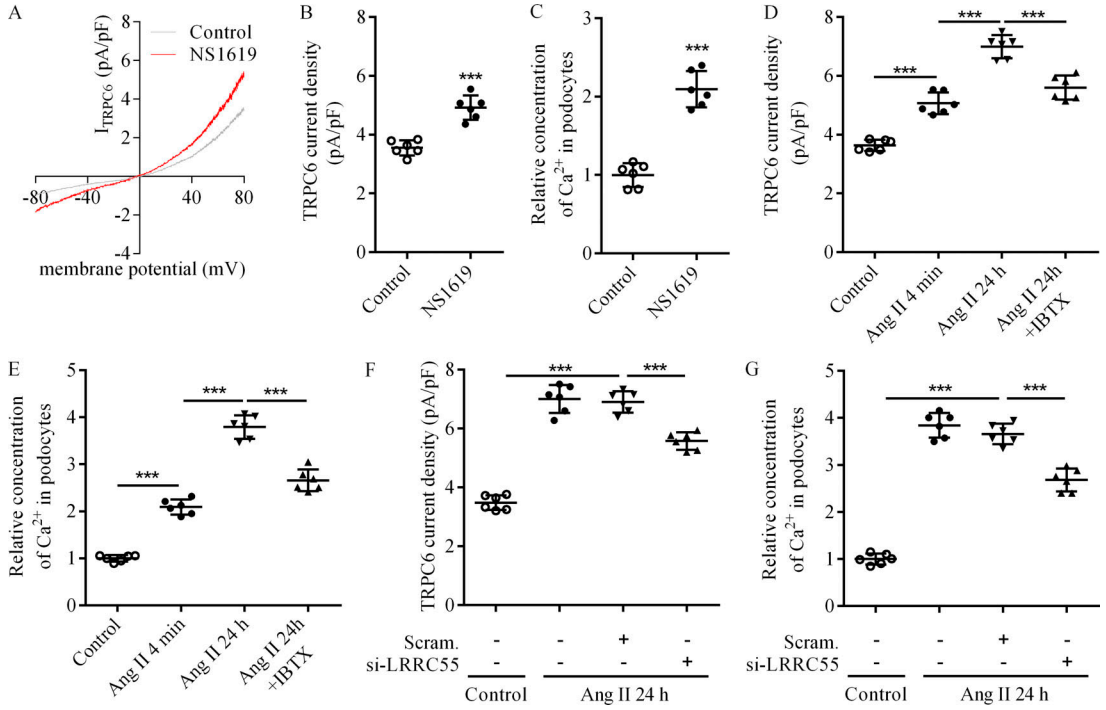

Figure S4. **Activation of the BK channel exacerbates TRPC6-mediated Ca^{2+} influx in podocytes. (A)** I/V relationship of TRPC6 current in podocytes treated with NS1619. **(B)** TRPC6 current measured at +80 mV in podocytes treated with NS1619 (n = 6). **(C)** Level of intracellular Ca^{2+} in podocytes treated with NS1619 (n = 6). **(D)** TRPC6 current measured at +80 mV in podocytes treated with Ang II and IBTX (n = 6). **(E)** Level of intracellular Ca^{2+} in podocytes treated with Ang II and IBTX (n = 6). **(F)** Effect of LRRC55 siRNA on TRPC6 current in podocytes treated with Ang II for 24 h (n = 6). **(G)** Effect of LRRC55 siRNA on intracellular Ca^{2+} in podocytes treated with Ang II for 24 h (n = 6). Data shown are representative of three experiments. For statistical analysis, a two-tailed Student's t test was used for B and C, and one-way ANOVA with Tukey's post hoc test was used for D–G. ***, P < 0.001. Scram., scrambled.

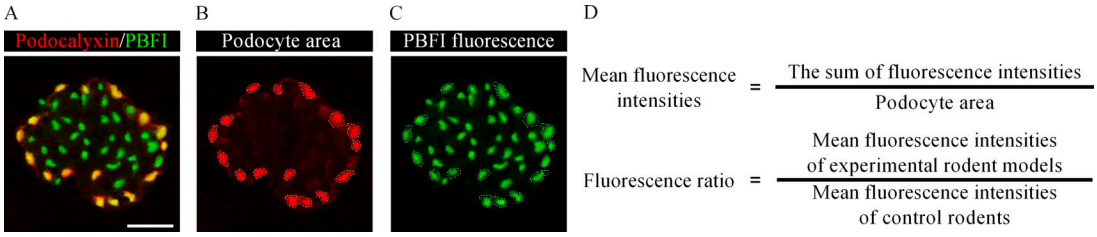

Figure S5. **Intracellular potassium assay in the podocytes of isolated rodent glomeruli in situ. (A)** Image of the PBFI-AM and a PE-conjugated podocalyxin antibody-loaded glomerulus. **(B)** The podocyte area selected according to the podocalyxin fluorescence signal. **(C)** Image used to determinate the PBFI fluorescence intensities in podocytes. **(D)** Calculation of the PBFI fluorescence ratio. Scale bar = 20 µm.

Table S1, Table S2, and Table S3 are provided online as separate Word documents. Table S1 provides the clinical and pathologic characteristics of the discovery and validation cohorts. Table S2 lists the primers used in this study. Table S3 lists the antibodies used in this study.